ABSTRACT

KWATRA, NITIN. Computation of Recruitment Volumes in the Human Body due to External Electric or Magnetic Stimulation using ADI-FDTD Method. (Under the direction of Prof. Gianluca Lazzi).

The Alternating-Direction Implicit Finite-Difference Time-Domain (ADI-FDTD) method is a computational electromagnetic method which, unlike the traditional explicit FDTD method, is unconditionally stable and allows arbitrarily large time steps. The decrease in the simulation time is achieved at the cost of accuracy. However, in computational problems where the results are averaging based, the effects of such local errors are largely minimized. For example, using ADI-FDTD in bioelectromagnetics, quantities like Specific Absorption Rates (SAR) and total induced currents can be computed over models with fine geometrical resolutions without decreasing the time step proportionally.

In this work, the volume of neurons excited (recruitment volume) inside a human body due to external electric or magnetic stimulation is computed using the D-H formulation of ADI-FDTD method. The electric stimulation considered is through current injection by contact electrodes of a Human Electro-Muscular Incapacitative (HEMI) device. For magnetic stimulation, two high frequency current pulses flowing in opposite directions in circular coils are considered. A neuron can be excited if the electric field or the gradient of the electric field along its length exceeds the nerve threshold value. These modes of excitation are termed as 'end mode' and 'center mode' respectively. The nerve excitation threshold values are decided based on experimental investigations on laboratory animals found in the literature.

Memory and simulation time requirements are reduced by employing expanding grid techniques and DFT averaging. The uniform grid of a 1 mm resolution model is logarithmically expanded to 5 mm in region far from source such as head, lower legs and arms. This reduces the computational size of the model by 90%. For HEMI current source stimulations, Discrete Fourier Transform (DFT) is used to find the induced electric fields due to the dominant frequencies in the current source. By using quasi-static assumptions, the DFT is evaluated for a duration substantially lesser than the time period of the different frequencies. The field values are then obtained as the ratios to the fields at the source and then scaled depending upon the magnitude of the source.

This study builds upon the efficient use of use of ADI-FDTD method for the solution of the low frequency bioelectromagnetic problems by employing expanding grid techniques and DFT averaging. Recruitment volumes due to a HEMI current source device are computed. A preliminary investigation on the use of magnetic stimulation for HEMI devices is also performed.

Computation of Recruitment Volumes in the Human Body due to External Electric or Magnetic Stimulation using ADI-FDTD Method

by
Nitin Kwatra

A thesis submitted to the Graduate Faculty of
North Carolina State University
in partial fullfillment of the
requirements for the Degree of
Master of Science

Electrical Engineering

Raleigh, North Carolina

2009

APPROVED BY:

Dr. G. Bilbro

Dr. J.K. Townsend

Dr. Gianluca Lazzi
Chair of Advisory Committee

DEDICATION

To my family

BIOGRAPHY

Nitin Kwatra received his Bachelor of Technology degree from Indian Institute of Technology - Guwahati in May 2005. He was a research assistant at the University of Zurich for one year where he worked EMG pattern recognition. He began his graduate studies at the North Carolina State University (NCSU) in fall 2007 and is presently a research assistant in the bio-electromagnetics lab under the guidance of Dr. Gianluca Lazzi. Nitin's research interests are bio-electromagnetics, bio-signal analysis and circuit design.

ACKNOWLEDGMENTS

I would like to thank Dr. Gianluca Lazzi for giving me the opportunity to work under his guidance. I owe my progress in this work to him for his knowledgable mentorship and the ever encouraging belief in me. His dedicated and disciplined approach to work is inspirational.

I was immensely helped by Ajeet in the initial days of my research. I am always grateful to him for helping me iron out the teething troubles. My discussions with Amit Qusba over simple to highly convolved issues helped me get a good grasp over basics and many a times led to novel ways to tackle research issues. I am grateful to Dr. Vinit Singh for always being receptive to my doubts and for clarifying them. I am also obliged to Dr. Gaurav Gupta for letting me confide in him. I am extremely indebted to Carlos Cela and Dr. Stefan Schmidt for their immense help in bolstering my research results. The closely knit research team of Dr. Lazzi has always been very approachable keeping the research experience very conducive.

Many thanks go to my room mates Saurabh, Sameer and Sidharth for making my stay at NCSU very enjoyable. Above all, I am immensely grateful to my family. I am highly obliged to my parents for a balanced brought up and my sisters for somewhat spoiling me. I am humbled by the patience, understanding and care shown by my wife Ruchi during my research and graduate studies.

TABLE OF CONTENTS

LIST OF TABLES

LIST OF FIGURES

Chapter 1

Introduction

1.1 HEMI devices and waveforms

Human Electro-Muscular Incapacitation (HEMI) devices are Non Lethal Weapons (NLW) used to temporarily immobilize a person by disrupting muscle control. NLWs are mainly used by law enforcement officials to bring about control in a violent situation like riots. The objective behind the use of a HEMI device is to avoid fatal bodily injury to a living subject while helping the user to bring about compliance while defending himself from a safe distance.

A typical HEMI device uses compressed nitrogen to propel two darts connected through insulated wires at a speed of about 48m/s. These darts go up to 10.5m from the user [1]. In 30% of the cases, these darts get stuck in the clothing of the target. In such an event, a transient 50kV electric arc is sent through the darts to break down any insulation like clothing or air between the skin and the darts. But such a high voltage is applied only until the darts make a contact with the conductive flesh [2]. Once the contact with the skin is established, current is injected through the darts in pulses. This current generates electric fields which capture motor nerves, which in

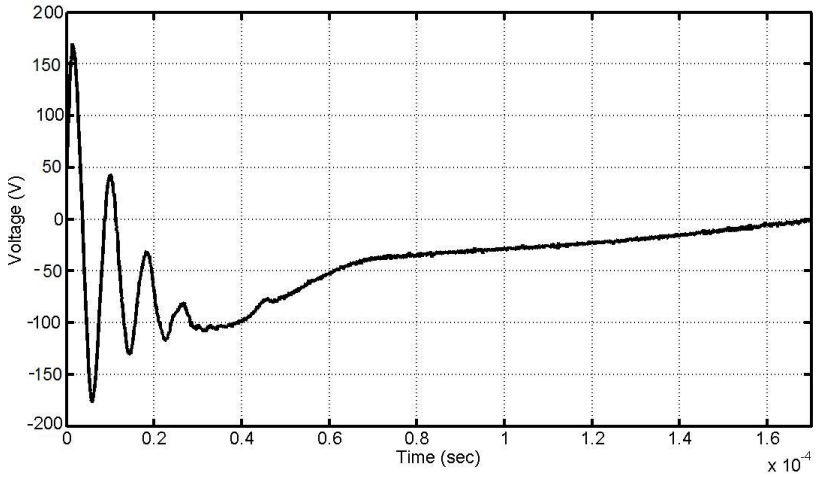

Figure 1.1: Pulse Waveform for X26 HEMI device

turn, may cause muscle contraction leading to impairment of locomotion.

As an example, it is described in [1] and [3] that a typical HEMI pulse for a X26 device with 50Ω load impedance has the waveform as shown in figure 1.1. The duration of this pulse is 0.17 millisecond with a peak current value of 3A [1]. It is intended to be a damped sinusoid with the fundamental frequency of 120KHz [3]. The waveform does not vary significantly with the change in load resistance as the HEMI devices are current sources, that is, they have high output impedance. It has been shown that the peak current changes only by 20% for a ten fold increase in load resistance from 470Ω to 4700Ω [3].

1.2 Neuromuscular Incapacitation and Recruitment volumes

The human brain controls the skeletal muscles which are responsible for all physical activities of a person like walking, talking and typing. The skeletal muscles

constitute around 40% of a typical human body mass. To contract a muscle, the brain sends an electric pulse through motor neurons to their terminal end at the middle of a muscle. This results in a molecular mechanism that contracts a muscle [3]. A HEMI device tries to circumvent the brain and cause the muscle contraction by itself.

Current injection through a HEMI device may cause muscle contraction and pain. The biological process underlying this could be direct muscle excitation, indirect muscles excitation through stimulation of motor neurons or reflex activity resulting from excitation of afferent neurons [4]. The correlation of the strength of muscle contraction at limbs with the volume in body where neurons are excited (recruitment volume) has been shown through experiments. It was found that as the separation between two electrodes increased, the extent of muscle contraction also increased. Beginning with a separation of 5cm, this continued up to 20cm, after which the strength of muscle contraction remained constant [5].

Neurons in the human body can be excited by the magnitude of the electric field or its gradient. These two modes of excitation are referred to as 'end mode' and 'center mode' respectively. A neuron is excited if the magnitude of the electric field or the gradient of the electric field along its length increases beyond the nerve excitation threshold value. Typically, these threshold values increase with decreasing neuron diameter or duration of stimulation [4].

When changing magnetic field is applied to a human body, electric fields and currents may be induced inside the body. Such fields may stimulate nerves and cause involuntary muscle contraction. Such contractions have been reported during MRI scans typically near prominently bony areas [6]. This motivates the investigation of the possibility of neuromuscular incapacitation through magnetic stimulation.

1.3 Motivation

HEMI devices are now being widely used world over by law enforcement agencies. With its ever increasing use, the public scrutiny of these devices over their safety has also elevated. The extent of muscle contraction may depend upon a number of things. For example, it depends upon the frequency at which the electric pulses are fired at the target. Such factors are extensively studied and constitute the specifications of a HEMI device [1].

As mention in section 1.2, the extent of muscle contraction appears to correlate with the recruitment volume. In this work, recruitment volumes in human body are computed for electric and magnetic stimulation and their distribution in the human body is studied. This research also lays the ground work for studying the effects of various factors like electrode cross section, its position and dielectric properties of the human tissue on recruitment volumes.

A number of numerical methods have been used to study the effects of low frequency electro-magnetic fields induced in a human body. Method of scaling is employed in [7] to simulate at 10MHz and scale results to 60Hz. Other methods such as impedance method [8] and Scalar Potential Finite Difference (SPFD) method [9] have also been used to compute induced electric and magnetic fields. What is notably lacking are the computational results depicting effects of specific HEMI waveforms. This very capability of Finite Difference Time Domain (FDTD) method to correctly model arbitrary HEMI waveform is highly instrumental in computing recruitment volumes and studying their distribution in the human body. In this research, we use D-H formulation of Alternate Direction Implicit FDTD (ADI-FDTD) method to compute recruitment volumes in a human body due to external electric and magnetic stimulations.

1.4 ADI FDTD Method

In bioelectromagnetics problems, such as the one at hand, the underlying model is typically over resolved. This puts a limit on the time step of a conventional FDTD method which is much more stringent than the one required to resolve the minimum signal wavelength. ADI-FDTD is specifically helpful in such cases as it is unconditionally stable and need not conform to the Courant-Freidrich-Lewy (CFL) limit. The factor by which the time step used in ADI-FDTD is more than the one dictated by CFL limit is called the CFL number or just CFLN. The acceleration in the simulation comes at the cost of accuracy [10] and computational memory requirements. Also, to get any reduction in computation time, the CFLN should be high enough. Bio-electromagnetic problems are highly tolerant to local inaccuracies as results are typically averaging based. For example, in calculating recruitment volumes, the regions in the body where the fields exceed certain threshold are required. In such scenarios, ADI-FDTD might be an effective and efficient way for numerical analysis [11].

1.5 Organization of Thesis

The organization of this thesis is as follows:

Chapter 2 discusses in detail the computational methods used in this research. The conventional FDTD method as proposed by Yee is described followed by its stability requirements. PML technique for the conventional FDTD as developed by Berenger is detailed followed by an introduction to the anisotropic PML which is the base for the PML used in this research. These basic theories lead to a discussion about the ADI-FDTD, its D-H formulation and PML implementation. Chapter 2 is concluded by discussing 3D expanding grid technique and DFT averaging technique which are

employed to reduce the simulation time. The computational results are presented in Chapter 3. First the human body models used in this research are presented along with their expanded grid counterparts. Next, the end mode and center mode recruitment volumes for both electric and magnetic stimulation are presented. Chapter 4 presents the conclusion and discusses the future work.

Chapter 2

Numerical Methods for Bioelectromagnetics

Bioelectromagnetics is the study of the interaction of electromagnetic fields with biological systems. One of the most common areas of investigation in bioelectromagnetics is the study of the impact of man made devices like cell phones, radios and power transmitters on humans. Computer based simulations are invaluable to such studies as analytical solutions are not possible.

Computational electromagnetics (CEM) in general, has helped scientists everywhere to solve Maxwell's equations to examine wave guiding, radiation and other technologies. Motivated by military defense applications and the advent of programmable digital computers, the initial approach to CEM was high-frequency asymptotic methods and integral equations [12]. The former of these frequency methods suffers from difficulty in treating material and structural complexity. Integral equations can overcome these issues but limits the electrical size of the models used, particularly of the ones with high geometrical details [12]. One of the most common integral methods used today is the Method of Moments (MOM) [13]. It should also be noted that

typically in a bioelectromagnetics problem, the underlying model is large, highly inhomogeneous and has a complex geometry making the above mentioned methods unsuitable in most cases.

Understanding of the limitations of frequency domain solutions as detailed above led to the increasing interest in direct solution of the Maxwell's difference equations. The first FDTD algorithm was proposed by Yee in 1966 [14] but it was not until 1970s and 1980s that its capabilities were realized. FDTD is robust, puts no limit on the electric size of the model, treats impulsive and non-linear behaviors naturally and treats complex geometries with ease. The error sources in FDTD are recognized and can be bounded [12]. All these qualities also make FDTD an invaluable technique for bioelectromagnetics problems.

The stability requirements of the FDTD algorithm puts a limit on the time step size that can be used for the simulation (CFL limit). This time step is directly proportional to the minimum grid spacing in the model. For most bioelectromagnetics problems, the grid spacing is generally very fine to inculcate the complexity of the underlying biological system. If the model is also large, this can result in an extremely slow simulation. Alternate Direction Implicit FDTD (ADI-FDTD) method circumvents this problem as it is unconditionally stable and does not need to conform to the CFL limit. The time step in ADI-FDTD is limited by accuracy instead of stability. Though the first time when ADI was applied to FDTD was in 1984 [15], the present form of ADI-FDTD was proposed by Zheng, Chen and Zhang in 2000 [16] along with the proof of its unconditional stability.

The FDTD method and all its derivatives also need to implement Absorbing Boundary Conditions (ABCs) to terminate the unbounded computational domains. An ideal ABC should accurately and efficiently absorb all incident waves at all incident angles and should not reflect any part of the incident waves back into the

computational domain. The introduction of the Perfectly Matched Layer (PML) by Berenger in 1994 [17] is widely considered to be the turning point in the development of efficient ABCs. There have been numerous papers validating Berenger's PML and proposing derivatives. The formulation used in this work was proposed by Lazzi in 2001 [18]. This D-H formulation of FDTD enables the PML conditions to be defined completely independent from the FDTD grid.

In the following sections, we discuss in detail the implementations of the FDTD algorithm, ADI-FDTD techniques, PMLs and other computational techniques used in this work.

2.1 The Finite-Difference Time-Domain Method

2.1.1 Yee's algorithm

The FDTD method for the solution of Maxwell's equations was developed by Kane Yee in 1966 [14]. Instead of solving just for either the electric ($\overrightarrow{E}$) or the magnetic field ($\overrightarrow{H}$), Yee's algorithm solves for both of them by interleaving them in time and space. The fields are staggered with respect to each other in time and space by half time step and half cell width respectively. The Yee cell shown in fig. 2.1 shows the fields interleaving in space. Each $\overrightarrow{E}$ component is surrounded by four circulating $\overrightarrow{H}$ components and each $\overrightarrow{H}$ component is surrounded by four circulating $\overrightarrow{E}$ components. The algorithm uses only Maxwell's curl equations which, in free space, are given as follows.

$$\frac{\partial E}{\partial t} = \frac{1}{\epsilon_0} \nabla \times H \tag{2.1}$$

$$\frac{\partial H}{\partial t} = -\frac{1}{\mu_0} \nabla \times E \tag{2.2}$$

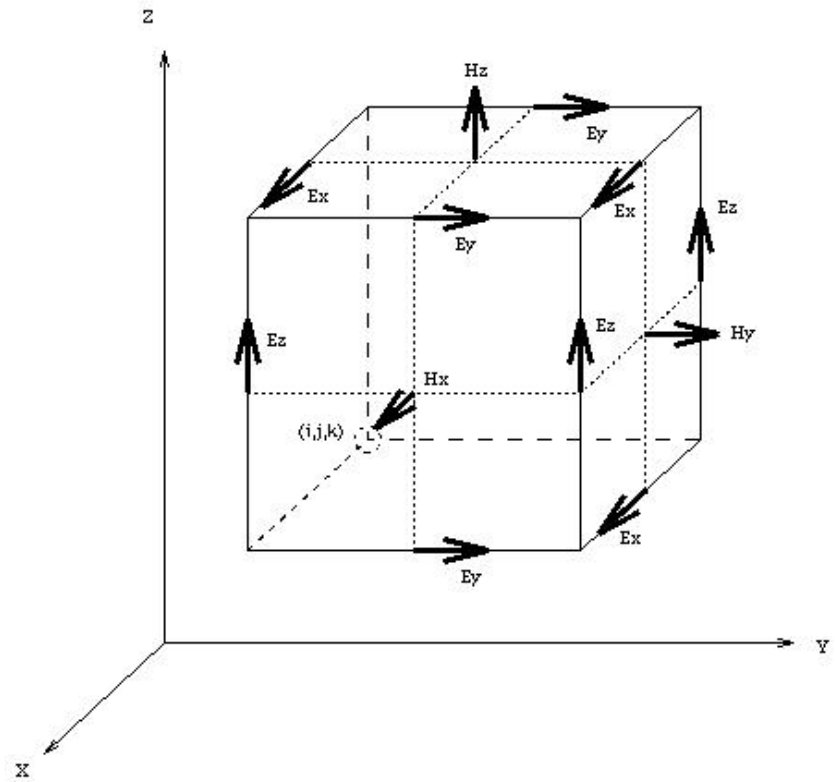

Figure 2.1: The E and H field components in Yee cell

The other two Maxwell equations are implicitly implied by the Yee cell through locations of the fields in the cell and by using central difference expressions for spatial gradient in the finite difference curl equations. Using both $\overrightarrow{E}$ and $\overrightarrow{H}$ makes the solution robust for a wider class of structures. The magnetic and electric properties of the material can also be easily modeled. [12].

The space and time interleaving can be easily understood using a simple case of one dimensional (1D) wave propagation. For a simple 1D case involving only E_x and H_y, the curl equations become [19]:

$$\frac{\partial E_x}{\partial t} = -\frac{1}{\epsilon_0}\frac{\partial H_y}{\partial z} \tag{2.3}$$

$$\frac{\partial H_y}{\partial t} = -\frac{1}{\mu_0}\frac{\partial E_x}{\partial z} \tag{2.4}$$

Both temporal and spacial derivatives are discretized using central difference approximations. This gives the following results

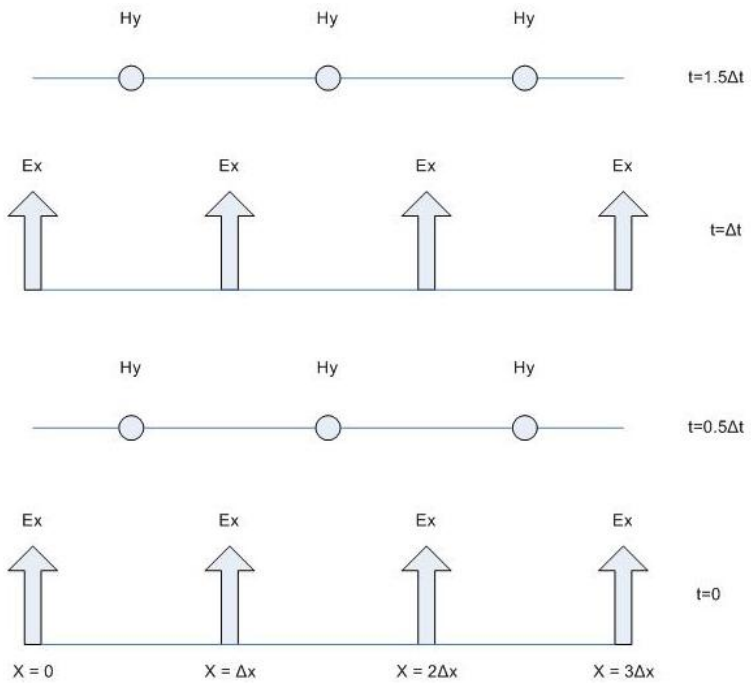

Figure 2.2: Space time interleaving for the Yee algorithm

$$\frac{E_x^{n+1/2}(k) - E_x^{n-1/2}(k)}{\Delta t} = -\frac{1}{\epsilon_0}\frac{H_y^n(k+1/2) - H_y^n(k-1/2)}{\Delta z} \tag{2.5}$$

$$\frac{H_y^{n+1}(k+1/2) - H_y^n(k+1/2)}{\Delta t} = -\frac{1}{\mu_0}\frac{E_x^{n+1/2}(k+1) - E_x^{n+1/2}(k)}{\Delta z} \tag{2.6}$$

The "n" superscripts refer to time $t = n \times \Delta t$ while the "k" terms in the parenthesis represents distance $z = k \times \Delta z$. Fig. 2.2 helps explain the leapfrog manner in which the FDTD algorithm proceeds. Let's assume that all the fields before $t = (n+1/2)\Delta t$ are known for all k. Then equation 2.5 gives E_x at $t = (n+1/2)\Delta t$ for all the k. These values can be used in equation 2.6 to find H_y at $t = (n+1)\Delta t$ for all the values of $(k+1/2)$. In the next step, these values are fed back to equation 2.5 to compute E_x at $t = (n+3/2)\Delta t$ which are again used in equation 2.6 to find H_y at $t = (n+2)\Delta t$. This goes on until the end of simulation when fields for all required n are computed.

2.1.2 Numerical Stability in Yee space model

For a long time domain simulation, we need the time step to be as large as possible. But the stability requirements constrain the maximum time step that can be used in a FDTD simulation. Consider a one dimensional wave propagation in a uniform grid of cell size Δx. Since an electromagnetic wave can not go faster than the speed of light c_0, the minimum time required to propagate one cell is $\Delta t = \frac{\Delta x}{c_0}$. For a n-dimensional space with uniform grid of Δx cell size, the stability condition is generalized by the famous Courant condition [19] [12] which is given by

$$\Delta t \leqslant \frac{\Delta x}{c_0\sqrt{n}} \tag{2.7}$$

If the minimum cell sizes in x, y and z directions are Δx, Δy and Δz respectively, the Courant condition can be generalized [12] as follows.

$$\Delta t \leq \frac{1}{c_0\sqrt{\frac{1}{\Delta x^2} + \frac{1}{\Delta y^2} + \frac{1}{\Delta z^2}}} \tag{2.8}$$

Care is also required in deciding the space cell size. The cell size should be able to resolve the underlying model as well as the shortest wavelength in the source signal. As a thumb rule, it is advisable to have at least 10 points per shortest wavelength [19].

In low frequency bioelectromagnetics problems, such as the one investigated in this research, the cell spacing is primarily decided by the model resolution and not by the shortest signal wavelength. For example, if the highest signal frequency is 120KHz, then the corresponding wavelength is 2500m. This allows for a cell spacing for 250m. This resolution can not possibly resolve human body models which are typically discretized at millimeter resolution.

2.1.3 Berenger's Perfectly Matched Layer

A number of Absorbing Boundary Conditions (ABCs) were being used before Berenger proposed the idea of the PML [17]. For most of the these earlier ABCs, the incident waves were absorbed perfectly only is special cases, for example when a plane wave was propagating perpendicular to the boundary. Berenger proposed a split field formulation to Maxwell's equation in two dimensions which could absorb an electromagnetic wave traveling with any angle of incidence, polarization or frequency. Berenger explained his idea in two dimension for a TE mode with no field variation in z direction and the PMLs enclosing the computational domain in x and y directions. For such a setup, Maxwell's curl equations for a general material with electrical conductivity σ and magnetic conductivity σ^* can be written as

$$\epsilon_0 \frac{\partial E_x}{\partial t} + \sigma E_x = \frac{\partial H_z}{\partial y} \tag{2.9}$$

$$\epsilon_0 \frac{\partial E_y}{\partial t} + \sigma E_y = -\frac{\partial H_z}{\partial x} \tag{2.10}$$

$$\mu_0 \frac{\partial H_z}{\partial t} + \sigma^* H_z = \frac{\partial E_z}{\partial y} - \frac{\partial E_y}{\partial x} \tag{2.11}$$

The impedance of this medium equals to that of vacuum if

$$\frac{\sigma}{\epsilon_0} = \frac{\sigma^*}{\mu_0} \tag{2.12}$$

and a plane wave travelings perpendicular to the boundary faces no reflection. Berenger's key manoeuvre of the curl equations above was to split the H_z field into two components: H_{zx} and H_{zy}. The new equations are as follows.

$$\epsilon_0 \frac{\partial E_x}{\partial t} + \sigma_y E_x = \frac{\partial (H_{zx} + H_{zy})}{\partial y} \tag{2.13}$$

$$\epsilon_0 \frac{\partial E_y}{\partial t} + \sigma_x E_y = -\frac{\partial (H_{zx} + H_{zy})}{\partial x} \tag{2.14}$$

$$\mu_0 \frac{\partial H_{zx}}{\partial t} + \sigma_x^* H_{zx} = -\frac{\partial E_y}{\partial x} \tag{2.15}$$

$$\mu_0 \frac{\partial H_{zy}}{\partial t} + \sigma_y^* H_{zy} = \frac{\partial E_x}{\partial y} \tag{2.16}$$

Berenger proved that if (σ_x, σ_x^*) and (σ_y, σ_y^*) individually satisfied equation 2.12, then for a wave with any angle the incidence, polarization or frequency, impedance of this medium matched that of vacuum to obviate reflection and the magnitude of the wave decreased exponentially inside the medium [17]. Berenger went on to propose scaling of the PML paramerters in the boundaries to mitigate discretization errors.

2.1.4 Anisotropic PML

Though Berenger's PML proved to be much more accurate than other ABCs used at that time [17], it had a drawback in modifying the Maxwell's equation to add degrees of freedom. This entailed considerable modification of the FDTD equations. A PML formulation without altering the Maxwell's equation was first proposed by Sacks et al. [20]. Since the loss terms in Berenger's PML were direction dependent, an anisotropic medium can be expected in this formulation.

The general Maxwell's equations for an anisotropic medium is given by the following equations [20].

$$\overrightarrow{\nabla}.[\overline{\epsilon}]\overrightarrow{E} = 0 \tag{2.17}$$

$$\overrightarrow{\nabla}.[\overline{\mu}]\overrightarrow{H} = 0 \tag{2.18}$$

$$\overrightarrow{\nabla} \times \overrightarrow{E} = -j\omega[\mu]\overrightarrow{H} - [\sigma_M]\overrightarrow{H} \tag{2.19}$$

$$\overrightarrow{\nabla} \times \overrightarrow{H} = j\omega[\epsilon]\overrightarrow{E} - [\sigma_E]\overrightarrow{E} \tag{2.20}$$

Here, $[\overline{\epsilon}]$ and $[\overline{\mu}]$ are complex tensors given by the following matrices.

$$[\overline{\epsilon}] = \epsilon_0 \begin{pmatrix} \epsilon_x + \frac{\sigma_E^x}{jw} & 0 & 0 \\ 0 & \epsilon_y + \frac{\sigma_E^y}{jw} & 0 \\ 0 & 0 & \epsilon_z + \frac{\sigma_E^z}{jw} \end{pmatrix} = \epsilon_0 \begin{pmatrix} a & 0 & 0 \\ 0 & b & 0 \\ 0 & 0 & c \end{pmatrix} = \epsilon_0[\Lambda] \tag{2.21}$$

$$[\overline{\mu}] = \mu_0 \begin{pmatrix} \mu_x + \frac{\sigma_M^x}{jw} & 0 & 0 \\ 0 & \mu_y + \frac{\sigma_M^y}{jw} & 0 \\ 0 & 0 & \mu_z + \frac{\sigma_M^z}{jw} \end{pmatrix} = \mu_0 \begin{pmatrix} a & 0 & 0 \\ 0 & b & 0 \\ 0 & 0 & c \end{pmatrix} = \mu_0[\Lambda] \tag{2.22}$$

To match the impedance of this medium to that of the free space, the following equation should be satisfied.

$$\frac{[\overline{\epsilon}]}{\epsilon_0} = \frac{[\overline{\mu}]}{\mu_0} \tag{2.23}$$

Sacks et al. showed that, for a two dimensional TE_y or TM_y case, a wave incident upon the anisotropic interface at $z = 0$ will not reflect and will be damped inside the medium if a,b and c are related by the following condition.

$$a = b = \frac{1}{c} \tag{2.24}$$

This formulation can be easily generalized for three dimensional problems [12]. In such a case, the tensor $[\Lambda]$ in equations 2.21 and 2.22 changes to the following.

$$[\Lambda_{3D}] = \begin{pmatrix} a_x^{-1} & 0 & 0 \\ 0 & a_x & 0 \\ 0 & 0 & a_x \end{pmatrix} \begin{pmatrix} a_y & 0 & 0 \\ 0 & a_y^{-1} & 0 \\ 0 & 0 & a_y \end{pmatrix} \begin{pmatrix} a_z & 0 & 0 \\ 0 & a_z & 0 \\ 0 & 0 & a_z^{-1} \end{pmatrix} \tag{2.25}$$

This formulation does not require to alter the Maxwell's equations and its primary advantage is the ease of implementation. This formulation is the base of the PML for D-H formulation of ADI-FDTD developed by Schmidt and Lazzi [21] which is used in this research. A description of this technique is detailed later in this chapter.

2.2 Alternating Direction Finite-Difference Time-Domain Method

2.2.1 The Zheng, Chen, Zhang algorithm

As explained in section 2.1.2 on numerical stability of FDTD methods, the time step for a FDTD simulation is constrained by Courant's stability condition as given by equation 2.8. It was also mentioned that in low frequency bioelectromagnetic problems, this time step constraint is typically limited by the geometric resolution of the underlying model. For large models, for example the full human body model used in this research, the total time steps required for simulating a single time period of sinusoidal source can be probatively large. For example, let us assume a source of 120KHz frequency or $8.33\mu s$ time period. If the computational model is discretized at 1mm resolution, the Courant stability condition limits the time step to be $1.9ps$. This gives total number of time steps required to simulate for a single time period of the source signal to be a whopping 4.3×10^6!!.

The above example accentuates the need to surpass the Courant stability limit. In 2000, Zheng, Chen and Zhang proposed the unconditionally stable Alternate Direction Implicit-FDTD (ADI-FDTD) method [16] for three dimensional FDTD problems. In ADI-FDTD, the time step in constrained by the numerical accuracy of the solution and not its stability. For the same accuracy as of a conventional FDTD, ADI-FDTD requires at least four times lesser number of time steps [16]. In this section, ADI-FDTD formulation by Zheng, Chen and Zhang is detailed as described in [16] and [12].

The vector curl equations as given by 2.1 and 2.2 can each be split up into three scalar partial differential equations corresponding to the three cartesian coordinates are shown below. The curl equation for H is split as:

$$\frac{\partial E_x}{\partial t} = \frac{1}{\epsilon}(\frac{\partial H_z}{\partial y} - \frac{\partial H_y}{\partial z}) \tag{2.26}$$

$$\frac{\partial E_y}{\partial t} = \frac{1}{\epsilon}(\frac{\partial H_x}{\partial z} - \frac{\partial H_z}{\partial x}) \tag{2.27}$$

$$\frac{\partial E_z}{\partial t} = \frac{1}{\epsilon}(\frac{\partial H_y}{\partial x} - \frac{\partial H_x}{\partial y}) \tag{2.28}$$

Similarly, the curl equations for E can be split as:

$$\frac{\partial H_x}{\partial t} = -\frac{1}{\mu}(\frac{\partial E_z}{\partial y} - \frac{\partial E_y}{\partial z}) \tag{2.29}$$

$$\frac{\partial H_y}{\partial t} = -\frac{1}{\mu}(\frac{\partial E_x}{\partial z} - \frac{\partial E_z}{\partial x}) \tag{2.30}$$

$$\frac{\partial H_z}{\partial t} = -\frac{1}{\mu}(\frac{\partial E_y}{\partial x} - \frac{\partial E_x}{\partial y}) \tag{2.31}$$

Assuming that all the fields are known at all the locations at the nth time step, the marching from nth time step to $(n+1)$th time step is broken into two sub steps. One from nth time step to $(n+1/2)$th time step and the other from $(n+1/2)$th time step to $(n+1)$th time step. The first sub step can be explained using the discretization of equation 2.26 as shown below.

$$\epsilon\left[\frac{E_x|^{n+1/2}_{i+1/2,j,k} - E_x|^{n}_{i+1/2,j,k}}{\Delta t/2}\right] = \frac{H_z|^{n+1/2}_{i+1/2,j+1/2,k} - H_z|^{n+1/2}_{i+1/2,j-1/2,k}}{\Delta y} - \frac{H_y|^{n}_{i+1/2,j,k+1/2} - H_y|^{n}_{i+1/2,j,k-1/2}}{\Delta z} \tag{2.32}$$

Here, the first partial derivative on the RHS of 2.26 in approximated implicitly while the second partial derivative is approximated explicitly. For the second sub step though, the first partial derivative on the RHS of 2.26 in approximated explicitly while the second partial derivative is approximated implicitly as shown below.

$$\epsilon\left[\frac{E_x|^{n+1}_{i+1/2,j,k}-E_x|^{n+1/2}_{i+1/2,j,k}}{\Delta t/2}\right]=\frac{H_z|^{n+1/2}_{i+1/2,j+1/2,k}-H_z|^{n+1/2}_{i+1/2,j-1/2,k}}{\Delta y}$$
$$-\frac{H_y|^{n+1}_{i+1/2,j,k+1/2}-H_y|^{n+1}_{i+1/2,j,k-1/2}}{\Delta z} \tag{2.33}$$

Once all the equations from 2.26 to 2.31 are discretized in this manner for the first sub step, the resulting linear system of equations form a tridiagonal matrix. These equations for the first sub step are detailed below.

$$\left[1+\frac{(\Delta t)^2}{2\mu\epsilon(\Delta y)^2}\right]E_x|^{n+1/2}_{i+1/2,j,k}-\left[\frac{(\Delta t)^2}{4\mu\epsilon(\Delta y)^2}\right]\left(E_x|^{n+1/2}_{i+1/2,j-1,k}+E_x|^{n+1/2}_{i+1/2,j+1,k}\right)$$
$$=E_x|^{n}_{i+1/2,j,k}+\frac{(\Delta t)}{2\epsilon\Delta y}\left(H_z|^{n}_{i+1/2,j+1/2,k}-H_z|^{n}_{i+1/2,j-1/2,k}\right)$$
$$-\frac{(\Delta t)}{2\epsilon\Delta z}\left(H_y|^{n}_{i+1/2,j,k+1/2}-H_y|^{n}_{i+1/2,j,k-1/2}\right)$$
$$-\left[\frac{(\Delta t)^2}{4\mu\epsilon\Delta y\Delta x}\right]\left(E_y|^{n}_{i+1,j+1/2,k}-E_y|^{n}_{i,j+1/2,k}-E_y|^{n}_{i+1,j-1/2,k}+E_y|^{n}_{i,j-1/2,k}\right) \tag{2.34}$$

$$\left[1+\frac{(\Delta t)^2}{2\mu\epsilon(\Delta z)^2}\right]E_y|^{n+1/2}_{i,j+1/2,k}-\left[\frac{(\Delta t)^2}{4\mu\epsilon(\Delta z)^2}\right]\left(E_y|^{n+1/2}_{i,j+1/2,k-1}+E_y|^{n+1/2}_{i,j+1/2,k+1}\right)$$
$$=E_y|^{n}_{i,j+1/2,k}+\frac{(\Delta t)}{2\epsilon\Delta z}\left(H_x|^{n}_{i,j+1/2,k+1/2}-H_x|^{n}_{i,j+1/2,k-1/2}\right)$$
$$-\frac{(\Delta t)}{2\epsilon\Delta x}\left(H_z|^{n}_{i+1/2,j+1/2,k}-H_z|^{n}_{i-1/2,j+1/2,k}\right)$$
$$-\left[\frac{(\Delta t)^2}{4\mu\epsilon\Delta y\Delta z}\right]\left(E_z|^{n}_{i,j+1,k+1/2}-E_z|^{n}_{i,j,k+1/2}-E_z|^{n}_{i,j+1,k-1/2}+E_z|^{n}_{i,j,k-1/2}\right) \tag{2.35}$$

$$\left[1+\frac{(\Delta t)^2}{2\mu\epsilon(\Delta x)^2}\right]E_z|^{n+1/2}_{i,j,k+1/2}-\left[\frac{(\Delta t)^2}{4\mu\epsilon(\Delta x)^2}\right]\left(E_z|^{n+1/2}_{i-1,j,k+1/2}+E_z|^{n+1/2}_{i+1,j,k+1/2}\right)$$
$$=E_z|^{n}_{i,j,k+1/2}+\frac{(\Delta t)}{2\epsilon\Delta x}\left(H_y|^{n}_{i+1/2,j,k+1/2}-H_y|^{n}_{i-1/2,j,k+1/2}\right)$$
$$-\frac{(\Delta t)}{2\epsilon\Delta y}\left(H_x|^{n}_{i,j+1/2,k+1/2}-H_x|^{n}_{i,j-1/2,k+1/2}\right)$$
$$-\left[\frac{(\Delta t)^2}{4\mu\epsilon\Delta x\Delta z}\right]\left(E_x|^{n}_{i+1/2,j,k+1}-E_x|^{n}_{i+1/2,j,k}-E_x|^{n}_{i-1/2,j,k+1}+E_x|^{n}_{i-1/2,j,k}\right) \tag{2.36}$$

$$H_x|^{n+1/2}_{i,j+1/2,k+1/2} = H_x|^{n}_{i,j+1/2,k+1/2} + \frac{(\Delta t)}{2\mu\Delta z}\left(E_y|^{n+1/2}_{i,j+1/2,k+1} - E_y|^{n+1/2}_{i,j+1/2,k}\right) - \frac{(\Delta t)}{2\mu\Delta y}\left(E_z|^{n}_{i,j+1,k+1/2} - E_z|^{n}_{i,j,k+1/2}\right) \quad (2.37)$$

$$H_y|^{n+1/2}_{i+1/2,j,k+1/2} = H_y|^{n}_{i+1/2,j,k+1/2} + \frac{(\Delta t)}{2\mu\Delta x}\left(E_z|^{n+1/2}_{i+1,j,k+1/2} - E_z|^{n+1/2}_{i,j,k+1/2}\right) - \frac{(\Delta t)}{2\mu\Delta z}\left(E_x|^{n}_{i+1/2,j,k+1} - E_x|^{n}_{i+1/2,j,k}\right) \quad (2.38)$$

$$H_z|^{n+1/2}_{i+1/2,j+1/2,k} = H_z|^{n}_{i+1/2,j+1/2,k} + \frac{(\Delta t)}{2\mu\Delta y}\left(E_x|^{n+1/2}_{i+1/2,j+1,k} - E_x|^{n+1/2}_{i+1/2,j,k}\right) - \frac{(\Delta t)}{2\mu\Delta x}\left(E_y|^{n}_{i+1,j+1/2,k} - E_y|^{n}_{i,j+1/2,k}\right) \quad (2.39)$$

Note the equation 2.34 for the E_x field computation at $(n + 1/2)$th time step. All the terms on the RHS are known. Writing down these equations by varying j and keeping i and k constant, the formation of a tridiagonal matrix can be easily observed. Similar matrix systems can be formed for computing E_y and E_z using 2.35 and 2.36. It must be noted that fast algorithms are available for computing solutions to tridiagonal matrices. A LU factorization based matrix inversion program provided by LAPACK is used in this research.

After computing the E fields values at $(n+1/2)$th time step, the H field values at $(n + 1/2)$th time step can be easily computed explicitly as shown in equations 2.37 through 2.39. Using the computationally expensive tridiagonal matrix inversion is not required for this.

In a similar way, field value at $(n+1)$th time step can be computed using equations 2.40 through 2.45 as shown below.

$$
\begin{aligned}
\left[1+\frac{(\Delta t)^2}{2\mu\epsilon(\Delta z)^2}\right] E_x\big|_{i+1/2,j,k}^{n+1} - \left[\frac{(\Delta t)^2}{4\mu\epsilon(\Delta z)^2}\right]\left(E_x\big|_{i+1/2,j,k-1}^{n+1} + E_x\big|_{i+1/2,j,k+1}^{n+1}\right) \\
= E_x\big|_{i+1/2,j,k}^{n+1/2} + \frac{(\Delta t)}{2\epsilon\Delta y}\left(H_z\big|_{i+1/2,j+1/2,k}^{n+1/2} - H_z\big|_{i+1/2,j-1/2,k}^{n+1/2}\right) \\
-\frac{(\Delta t)}{2\epsilon\Delta z}\left(H_y\big|_{i+1/2,j,k+1/2}^{n+1/2} - H_y\big|_{i+1/2,j,k-1/2}^{n+1/2}\right) \\
-\left[\frac{(\Delta t)^2}{4\mu\epsilon\Delta x\Delta z}\right]\left(E_z\big|_{i+1,j,k+1/2}^{n+1/2} - E_z\big|_{i,j,k+1/2}^{n+1/2} - E_z\big|_{i+1,j,k-1/2}^{n+1/2} + E_z\big|_{i,j,k-1/2}^{n+1/2}\right)
\end{aligned} \tag{2.40}
$$

$$
\begin{aligned}
\left[1+\frac{(\Delta t)^2}{2\mu\epsilon(\Delta x)^2}\right] E_y\big|_{i,j+1/2,k}^{n+1} - \left[\frac{(\Delta t)^2}{4\mu\epsilon(\Delta x)^2}\right]\left(E_y\big|_{i-1,j+1/2,k}^{n+1} + E_y\big|_{i+1,j+1/2,k}^{n+1}\right) \\
= E_y\big|_{i,j+1/2,k}^{n+1/2} + \frac{(\Delta t)}{2\epsilon\Delta z}\left(H_x\big|_{i,j+1/2,k+1/2}^{n+1/2} - H_x\big|_{i,j+1/2,k-1/2}^{n+1/2}\right) \\
-\frac{(\Delta t)}{2\epsilon\Delta x}\left(H_z\big|_{i+1/2,j+1/2,k}^{n+1/2} - H_z\big|_{i-1/2,j+1/2,k}^{n+1/2}\right) \\
-\left[\frac{(\Delta t)^2}{4\mu\epsilon\Delta x\Delta y}\right]\left(E_x\big|_{i+1/2,j+1,k}^{n+1/2} - E_x\big|_{i+1/2,j,k}^{n+1/2} - E_x\big|_{i-1/2,j+1,k}^{n+1/2} + E_x\big|_{i-1/2,j,k}^{n+1/2}\right)
\end{aligned} \tag{2.41}
$$

$$
\begin{aligned}
\left[1+\frac{(\Delta t)^2}{2\mu\epsilon(\Delta y)^2}\right] E_z\big|_{i,j,k+1/2}^{n+1} - \left[\frac{(\Delta t)^2}{4\mu\epsilon(\Delta y)^2}\right]\left(E_z\big|_{i,j-1,k+1/2}^{n+1} + E_z\big|_{i,j+1,k+1/2}^{n+1}\right) \\
= E_z\big|_{i,j,k+1/2}^{n+1/2} + \frac{(\Delta t)}{2\epsilon\Delta x}\left(H_y\big|_{i+1/2,j,k+1/2}^{n+1/2} - H_y\big|_{i-1/2,j,k+1/2}^{n+1/2}\right) \\
-\frac{(\Delta t)}{2\epsilon\Delta y}\left(H_x\big|_{i,j+1/2,k+1/2}^{n+1/2} - H_x\big|_{i,j-1/2,k+1/2}^{n+1/2}\right) \\
-\left[\frac{(\Delta t)^2}{4\mu\epsilon\Delta y\Delta z}\right]\left(E_y\big|_{i,j+1/2,k+1}^{n} - E_y\big|_{i,j+1/2,k}^{n} - E_y\big|_{i,j-1/2,k+1}^{n} + E_x\big|_{i,j-1/2,k}^{n}\right)
\end{aligned} \tag{2.42}
$$

$$
\begin{aligned}
H_x\big|_{i,j+1/2,k+1/2}^{n+1} = H_x\big|_{i,j+1/2,k+1/2}^{n+1/2} + \frac{(\Delta t)}{2\mu\Delta z}\left(E_y\big|_{i,j+1/2,k+1}^{n+1/2} - E_y\big|_{i,j+1/2,k}^{n+1/2}\right) \\
-\frac{(\Delta t)}{2\mu\Delta y}\left(E_z\big|_{i,j+1,k+1/2}^{n+1} - E_z\big|_{i,j,k+1/2}^{n+1}\right)
\end{aligned} \tag{2.43}
$$

$$H_y|_{i+1/2,j,k+1/2}^{n+1} = H_y|_{i+1/2,j,k+1/2}^{n+1/2} + \frac{(\Delta t)}{2\mu\Delta x}\left(E_z|_{i+1,j,k+1/2}^{n+1/2} - E_z|_{i,j,k+1/2}^{n+1/2}\right) - \frac{(\Delta t)}{2\mu\Delta z}\left(E_x|_{i+1/2,j,k+1}^{n+1} - E_x|_{i+1/2,j,k}^{n+1}\right) \quad (2.44)$$

$$H_z|_{i+1/2,j+1/2,k}^{n+1} = H_z|_{i+1/2,j+1/2,k}^{n+1/2} + \frac{(\Delta t)}{2\mu\Delta y}\left(E_x|_{i+1/2,j+1,k}^{n+1/2} - E_x|_{i+1/2,j,k}^{n+1/2}\right) - \frac{(\Delta t)}{2\mu\Delta x}\left(E_y|_{i+1,j+1/2,k}^{n+1} - E_y|_{i,j+1/2,k}^{n+1}\right) \quad (2.45)$$

The factor by which the time step used in an ADI-FDTD method is more than the maximum possible in a conventional FDTD method is called the Courant-Freirich-Lewy (CFL) number or just CFLN. As mentioned before in chapter 1, ADI-FDTD is computationally more expensive than conventional FDTD. Hence it is wrong to perceive that ADI-FDTD with a CFLN of 4 will lead to a speed up of 4 in simulation time over the conventional FDTD. For the problem set up in this research, it was observed that a CFLN of 4 gave almost no gain in simulation time. Hence a CFLN of 16 was used.

2.2.2 PML in D-H formulation for ADI FDTD

The equations for anisotropic PML discussed in section 2.1.4 do not separate the background material from the PML layer. This is conspicuous form Equations 2.17 through 2.20. The PML condition is not independent of the background material and and there is no straight forward way to have any part of the background material inside the PML. Sometimes, when the model size gets bigger or when the modeled geometry is infinite in a dimension (for example a long transmission line), it is required to immerse the background material into the PML. D-H formulation allows to do just that. The PML in the D-H formulation for the conventional FDTD was proposed by

Sullivan in 1996 [22]. For ADI-FDTD, Lazzi proposed PML in D-H formulation in 2001 [18]. Unfortunately, this formulation suffered from substantial reflection errors from the corner cells. More so, these errors increased with the CFL number. To rectify this isssue, Schmidt and Lazzi published a better D-H formulation in 2003 [21]. This formulation is detailed below along with the basics of a D-H formulation.

Consider the following normalized Maxwell's equations.

$$j\omega\overrightarrow{D} = c_0.\nabla \times \overrightarrow{H} \tag{2.46}$$

$$\overrightarrow{D}(\omega) = \epsilon_r(\omega)\overrightarrow{E} \tag{2.47}$$

$$j\omega\overrightarrow{H} = -c_0.\nabla \times \overrightarrow{E} \tag{2.48}$$

Writing the scalar partial differential equation for the D_x field component from 2.46 with PML conductivity profiles in x, y and z directions, following equation is attained:

$$j\omega D_x \left(1 + \frac{\sigma_x^{PML}(x)}{j\omega\epsilon_0}\right)^{-1} \left(1 + \frac{\sigma_y^{PML}(y)}{j\omega\epsilon_0}\right) \left(1 + \frac{\sigma_z^{PML}(z)}{j\omega\epsilon_0}\right) = c_0 \left(\frac{\partial H_z}{\partial y} - \frac{\partial H_y}{\partial z}\right) \tag{2.49}$$

A similar equation can be written for H field components using 2.48. The background material properties are confined to 2.47. Note that the PML conductivity profiles and the background material properties are completely independent allowing immersing of the modeled geometry into the PML.

As detailed in section 2.2, ADI time stepping is divided amongst two sub steps of half a time step each. When equation 2.49 is discretized for the first sub step, the following equation is obtained [21]:

$$D_x^{n+1/2} = \frac{P_y^{N1} P_z^{N1}}{P_y^D P_z^D} D_x^n - 4 \frac{P_y^{N2} P_z^{N2}}{P_y^D P_z^D} \sum_{s=1/2}^{n} D_x^s + c_0 \Delta t$$

$$\left[\frac{P_x^{N3}}{P_y^D P_z^D} \frac{\partial H_z^{n+1/2}}{\partial y} - \frac{P_x^{N4}}{P_y^D P_z^D} \frac{\partial H_y^n}{\partial z} + 2 \frac{P_x^{N5}}{P_y^D P_z^D} \sum_{s=1/2}^{n} \left(\frac{\partial H_z^s}{\partial y} - \frac{\partial H_y^s}{\partial z} \right) \right] \tag{2.50}$$

The same equation discretized for the second half step gives

$$D_x^{n+1} = \frac{P_y^{N1} P_z^{N1}}{P_y^D P_z^D} D_x^{n+1/2} - 4 \frac{P_y^{N2} P_z^{N2}}{P_y^D P_z^D} \sum_{s=1/2}^{n+1/2} D_x^s + c_0 \Delta t$$

$$\left[\frac{P_x^{N4}}{P_y^D P_z^D} \frac{\partial H_z^{n+1/2}}{\partial y} - \frac{P_x^{N3}}{P_y^D P_z^D} \frac{\partial H_y^n}{\partial z} + 2 \frac{P_x^{N5}}{P_y^D P_z^D} \sum_{s=1/2}^{n+1/2} \left(\frac{\partial H_z^s}{\partial y} - \frac{\partial H_y^s}{\partial z} \right) \right] \tag{2.51}$$

Where,

$$P_x^D = P_x^{N3} = 1 + \frac{\sigma_x^{PML} \Delta t}{2\epsilon_0} = 1 + X_n(i)$$

$$P_x^{N1} = P_x^{N4} = 1 - \frac{\sigma_x^{PML} \Delta t}{2\epsilon_0} = 1 - X_n(i)$$

$$P_x^{N2} = P_x^{N5} = \frac{\sigma_x^{PML} \Delta t}{2\epsilon_0} = X_n(i) \tag{2.52}$$

As mentioned in section 2.2, H field components can be computed explicitly. For the second sub step, H_z can be computed as [21]:

$$H_z^{n+1} = \frac{P_x^{N1} P_y^{N1}}{P_y^D P_x^D} H_z^{n+1/2} - 4 \frac{P_x^{N2} P_y^{N2}}{P_x^D P_y^D} \sum_{s=1/2}^{n+1/2} H_z^s + c_0 \Delta t$$

$$\left[\frac{P_z^{N4}}{P_x^D P_y^D} \frac{\partial E_x n + 1/2}{\partial y} - \frac{P_z^{N3}}{P_x^D P_y^D} \frac{\partial E_y n + 1}{\partial x} + 2 \frac{P_z^{N5}}{P_x^D P_y^D} \sum_{s=1/2}^{n+1/2} \left(\frac{\partial E_x s}{\partial y} - \frac{\partial E_y s}{\partial x} \right) \right] \tag{2.53}$$

Finally, using the scalar partial differential equation for the y component of E from 2.47, the finite difference equation for computing E from D is as follows [21].

$$E_y^{n+1} = \frac{\left(D_y^{n+1} - \frac{\sigma_y \Delta t}{\epsilon_0} \sum_{s=1/2}^{n+1/2} E_y^s\right)}{\epsilon_{r,y} + \frac{\sigma_y \Delta t}{2\epsilon_0}} \tag{2.54}$$

Equation 2.54 can be substituted into 2.53 which can finally be substituted into 2.51 to result in a tridiagonal matrix system which is the characteristic of the ADI scheme. This matrix can be easily solved using LH factorization based matrix inversion. Similarly, other components of D can be computed as well. Following this, H fileds can be computed explicitly.

2.3 Expanding grid technique for FDTD method

For large models with high resolutions, the number of cells in the model becomes extremely huge. For example, the human body model used in this research is discretized at 1mm resolution and the total number of cells for this model is 374 million approximately. FDTD methods run over such models correspond to unrealistically long simulation times and memory requirements. It should also be noted that typically, not all the areas in the body are of primary importance. Also, not all the parts of the underlying model are highly coupled to the electromagnetic fields. For example, the human model used is this research is excited from near the chest and the belly. The fields, in such a case, remain coupled mainly in the torso region. Also, the area outside the body, which is air and the PML, also constitutes a big part of the total number of cells in computational grid. Such areas which contribute to the quantities of interest in negligible amount, if any, end up using a substantial portion of the computational resources.

To counter this issues, Gao and Gandhi proposed an expanding grid scheme in

which the cells remain at high resolution near the area of primary interest or the area where the coupling with the fields is substantial. On moving away from this specific area, the cell size increases exponentially [23]. The cell sizes must still be able to resolve the minimum wavelength of the source signal(cell size $< \lambda_{min}/10$). The expansion factors (α) could be different for the three axes. α of the order of 1.03 to 10.8 was found to have excellent agreement with analytical results for 2D lossy cylinders and 3D homogenous spheres [23]. The expanding grid method is invaluable to many application. For example, in the presence of reflecting boundaries distant from a near source, the near field can be modeled at higher resolution than the reflecting boundaries. For the human body model used in this research, the total cell number was reduced to 30 million from 374 million, a reduction of almost 90%. Details of this reduction can be found in later chapters.

To obtain an expanding grid model, a uniform high resolution model is started with. Then, the smallest cell size (δ_{min}) and the largest cell size (δ_{max}) are decided along with the expansion factor α. The selection of the high resolution area in the model thereafter ascertains the expanding grid cell boundaries. An expanded grid cell will now contain one or more of the high resolution cells. The type of the former is decided by the maximum number of a particular type of high resolution cells it contains.

2.4 Quasi static assumption and DFT averaging

As explained in the preceding sections, a number of techniques were employed to reduce the simulation time for the problem at hand. First, ADI-FDTD was used with a CFLN of 16 to circumvent the Courant stability limit and increase the time-step of the algorithm from $\approx 2ps$ to $\approx 30ps$. For a problem with an underlying model as

big as a full human body model discretized at 1mm resolution and amounting to a total computational cell count of almost 370 million, just increasing the time step was clearly not enough. Using expanding grid technique, the number of computational cells was reduced from 370 million to 30 million. As an example, the waveform of the HEMI X26 device [1], [3] with a time length of $\approx 0.17ms$ was used. With a time step of 30ps, the number of steps required for this simulation would be $0.17ms/30ps \approx 5.6 \times 10^6$. The number of days such a setup would take on a typical 2GHz Opteron based computer is around 5000 which is unacceptably long. It was mentioned in chapter 1 that the X26 waveform used as an example here, can be re-constructed from 27 harmonics of the base 120KHz signal. Simulating for a single time period of this frequency could also be considered, but the number of time steps required would still remain as high as 300,000.

To get around this roadblock, quasi-static conditions were assumed which allow Discrete Fourier Transform (DFT) to find average field values at the desired frequencies. Two condition must be satisfied for quasi-static assumptions to be valid[24]:

1. The model dimension should be much smaller than the smallest effective wavelength.

2. Conduction currents should be sufficiently larger than the displacement currents ($\sigma >> \omega\epsilon$).

Both these conditions are satisfied in the case studied here as the stimulus frequency content is less than 200 KHz. Hence, differences in phase can been neglected.

DFT was used to obtain field values at the desired frequencies by averaging for time durations much shorter than the the time period of the frequencies constituting the source signal. For the setup of the current source, two electrodes with a finite gap enter the human body model. The field values in the body are normalized with

respect to the field at the finite gap.

$$F(i,j,k) = \frac{\sum^{t1} E_{i,j,k}(t)e^{-j\omega t}}{\sum^{t1} E_{source}(t)e^{-j\omega t}}, \tag{2.55}$$

Here, $F(i,j,k)$ depicts the ratio of the field value at an observation point in the body, t1 is the time over which the DFT in computed and ω is the angular frequency at which the result is desired. After the computation of these ratios at desired frequencies, the fields in the body can be scaled up by the magnitude of corresponding frequency component of the source signal. It was observed that the fields induced at various frequencies up to 200KHz are identical which assures the correctness of quasi static assumption.

2.5 Validation

The methods used in this research were validated in three ways. The first two were performed by Ajeet in [25] and are summarized below.

1. First, the conventional FDTD method was compared to the D-H ADI-FDTD method with CFLN 16 used in this research. Both the methods were run over the same body model of uniform 5mm resolution for 1 MHz source frequency. This frequency was chosen to be much higher than the ones used in this research in order to reduce the simulation time. On comparing the single voxel field values for the two methods, the maximum difference of the order of 20% was observed near the metal tissue interface [25]. Majority of the local maxima in field value differences were observed to be near areas with abrupt changes in tissue properties. Such accuracy errors for ADI near points with abrupt changes in field values have been reported [10] and are expected. It must be noted such errors are limited to only a few voxels and in this research, the computed

quantities are not single voxel dependent. Such local errors have little impact on averaged quantities computed in this research like DFT averaged fields and threshold based volumes.

2. Errors induced due to expanding grid D-H ADI-FDTD method are studied by comparing it with the uniform grid D-H ADI-FDTD method. The base model chosen for this simulation was the torso part cut out from the full human body model. The resulting 280×300×400 size model was reduced almost 10 times using expanding grid technique to the dimensions 144×152×153. An average relative error of just 1.9% was observed near the metal-tissue interface [25].

3. The DC resistance offered by the body using D-H ADI-FDTD method was compared to the one computed using a multi resolution impedance method [26]. The base model used in this method was the 1mm uniform resolution human body model. This model was passed through a multi resolution algorithm to form larger voxels out of homogenous parts of the model, though no voxel was allowed to grow beyond 32 mm side. The DC resistance found using this scheme was 1.96kΩ. This closely matched the DC resistance of 1.84kΩ obtained through D-H ADI-FDTD method.

Chapter 3

Results

3.1 Full-body human model

The base anatomical computational model employed in this research is a 1mm resolution model from the *Visible Human Project* [27]. As mentioned in chapter 2, the number of total computation cells for this model is extremely high. Hence, this base model was re-discretized using an expanding grid scheme.

3.1.1 Model set up for electrical stimulation

Fig. 3.1 shows the expanding grid profile that resulted in the reduction of the voxel count of the 1mm resolution model by about 90%. The resolution near the electrodes was maintained at 1mm. This resolution was gradually increases with an

Table 3.1: Details for the original and expanded grid models

Model	Minimum Resolution	Dimensions	Voxels
Original	1 mm	586×340×1878	∼370 million
Expanded grid	5 mm	251×178×687	∼30 million

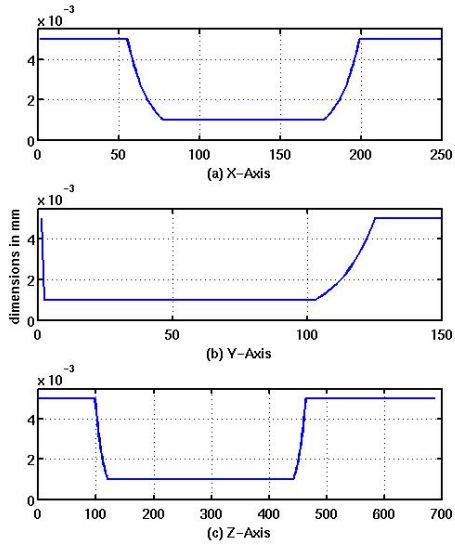

Figure 3.1: The expanding grid profiles without the PML (a) along the x-axis, (b) along the y-axis, and (c) along the z-axis.

expansion factor α of 1.095. The size details for the two model are give in table 3.1. Fig. 3.2 shows the expanding grid profiles laid on the base human body model. The lines are closely packed together and are dense in the areas of higher resolution near the signal source. They get farther apart gradually on moving away from the signal source.

Fig. 3.3 illustrates the positioning of the electrodes on the human torso for the electrical stimulation. The electrodes were placed almost 20 cm apart and penetrate about 10 cm into the body. The cross sectional area of the electrodes is 1 mm^2. Fig. 3.4 shows anatomical details of the original model. The dielectric properties of the human body tissues were obtained through an online data resource [28] which has been compiled by Gabriel et al. It must also be noted, that for the frequency range of interest (5.5 KHz - 156.6 KHz), the conductivities of most of the human body tissues vary by less than 5%. Also, the frequency dependence of the tissue properties has not been considered since the displacement current can be neglected at these frequencies.

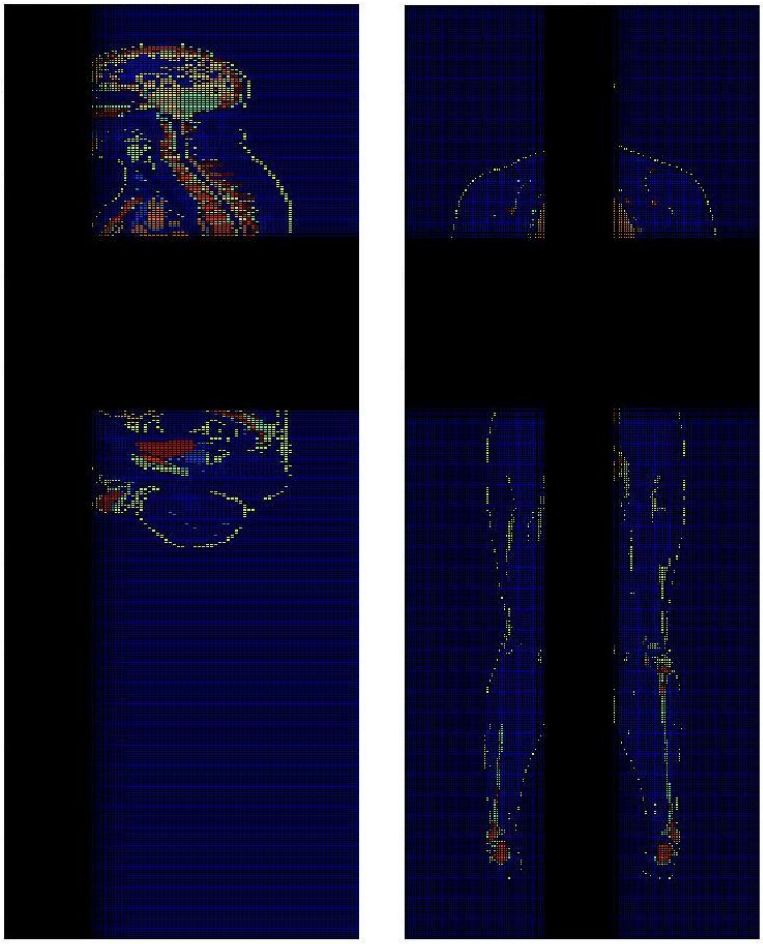

Figure 3.2: The expanding grid lines over the base human model with the PML (a) along the x-axis ans z-axis, (b) along the y-axis

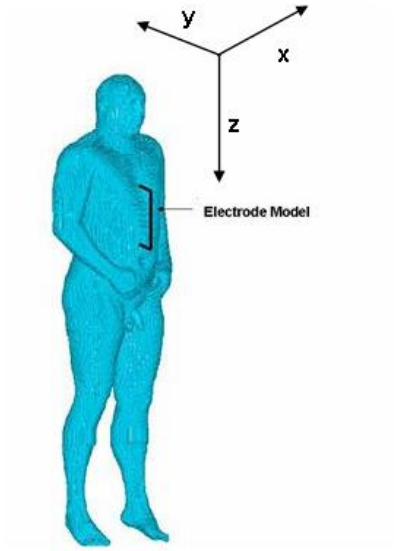

Figure 3.3: Computational model of the human body with the contact electrodes. The vertical distance between the electrode contacts is 20 cm.

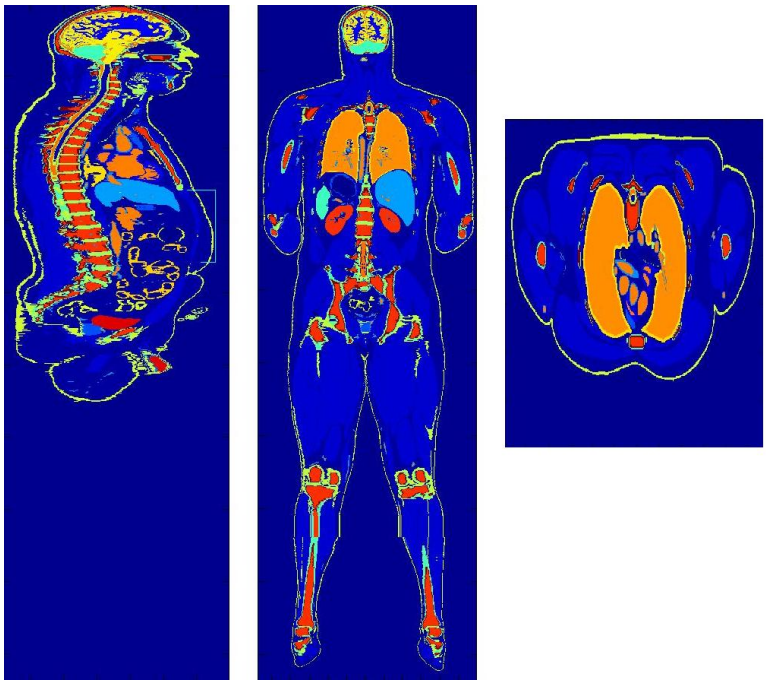

Figure 3.4: Anatomical details of the human body model.

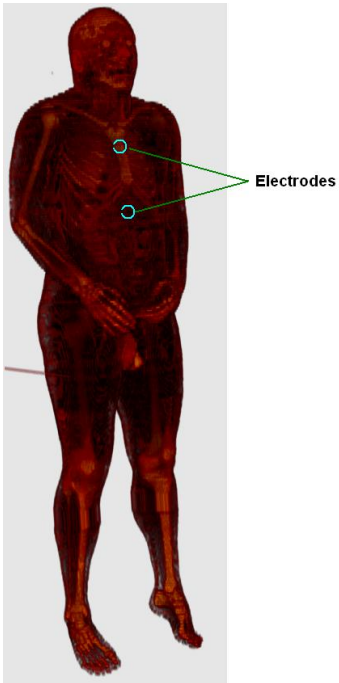

Figure 3.5: Electrode positioning over the human body model for magnetic stimulation

3.1.2 Model set up for magnetic stimulation

For magnetic stimulation set up, the 1mm uniform resolution model was shrunk using the expanding grid algorithm. The size details of the original and the expanded grid models are given in table 3.2. The electrodes for magnetic stimulation are two coils of 16mm diameter separated by 20cm from each other. The positioning of these coils is shown in fig. 3.5. The grid profiles for the grid expansion are shown in fig. 3.6.

Table 3.2: Details for the original model and the expanded grid model for magnetic stimulation

Model	Minimum Resolution	Dimensions	Voxels
Original	1 mm	586×340×1878	∼370 million
Expanded grid	5 mm	236×200×686	∼32 million

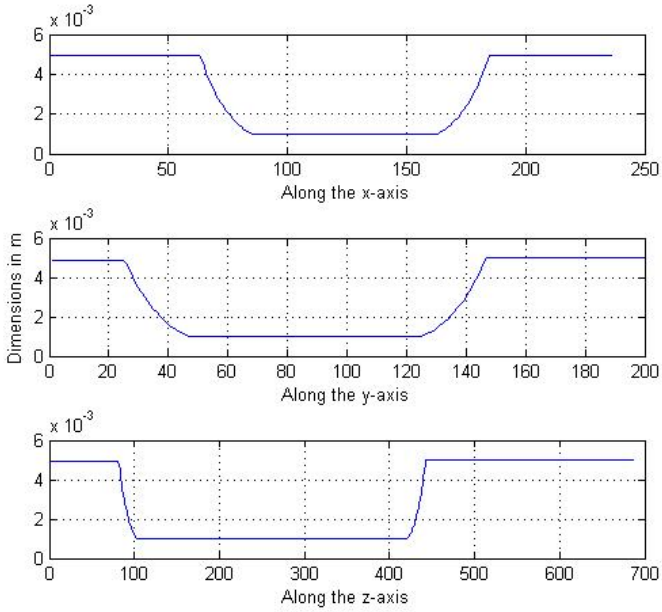

Figure 3.6: The expanding grid profiles of the human body model used for magnetic stimulation (a) along the x-axis, (b) along the y-axis, and (c) along the z-axis.

3.2 Recruitment volume for electrical stimulation

3.2.1 Computation of induced electric fields

The electric fields inside the body were normalized with respect to the field value at the source which is the finite gap between the electrodes. For the calculation of recruitment volumes, an excitation current I_{SRC} of 500mA was considered as it is the effective current for steady state duration in typical HEMI waveforms. The normalized field is scaled up by the magnitude of the field at the source corresponding to I_{SRC} flowing through the electrodes. The actual excitation current waveform used for the simulation was gaussian is shape which contained frequencies up to several 100 KHz. The results were computed at 120KHz using DFT averaging as detailed in chapter 2. The resistance offered by the body at 120KHz was approximated by the

one at DC. The DC resistance (R_{DC}) faced by the electrodes was computed as the ratio of the average voltage to the average current at the finite gap as shown below.

$$R_{DC} = \frac{\Sigma^{t1} V(t)}{\Sigma^{t1} I(t)} \tag{3.1}$$

Here t1 is the time up to which the average is computed while V(t) and I(t) are the time dependent voltage and current respectively at the source. The value of R_{DC} was found to be 1.84kΩ. This corresponds to an electric field E_{SRC} at the source given by:

$$\begin{aligned} E_{SRC} &= I_{SRC} \times R_{DC}/\Delta_{SRC} \\ &= 0.5A \times 1.84k\Omega/1mm \\ &= 9.2 \times 10^5 V/m \end{aligned} \tag{3.2}$$

Here, Δ_{SRC} is the cell size of the finite gap at the source. All the normalized fields were scaled up by the factor in (3.2) which is equal to 9.2×10^5.

The induced fields are shown in fig. 3.7. The fields are shown for a source current magnitude of 500mA. As expected, the electric fields are maximum near the points of contact of the electrodes. The fields drop substantially on moving away from the point of contact. The fields above the neck and in the lower legs are lower by a factor of 100.

3.2.2 End mode recruitment volume computation

As explained in section 1.2, the neurons in the human body can be excited if the magnitude of the electric field or its gradient along the length of a neuron exceeds the nerve excitation threshold value. The former mode of excitation is termed as 'end mode excitation' and its computation will be detailed in this section.

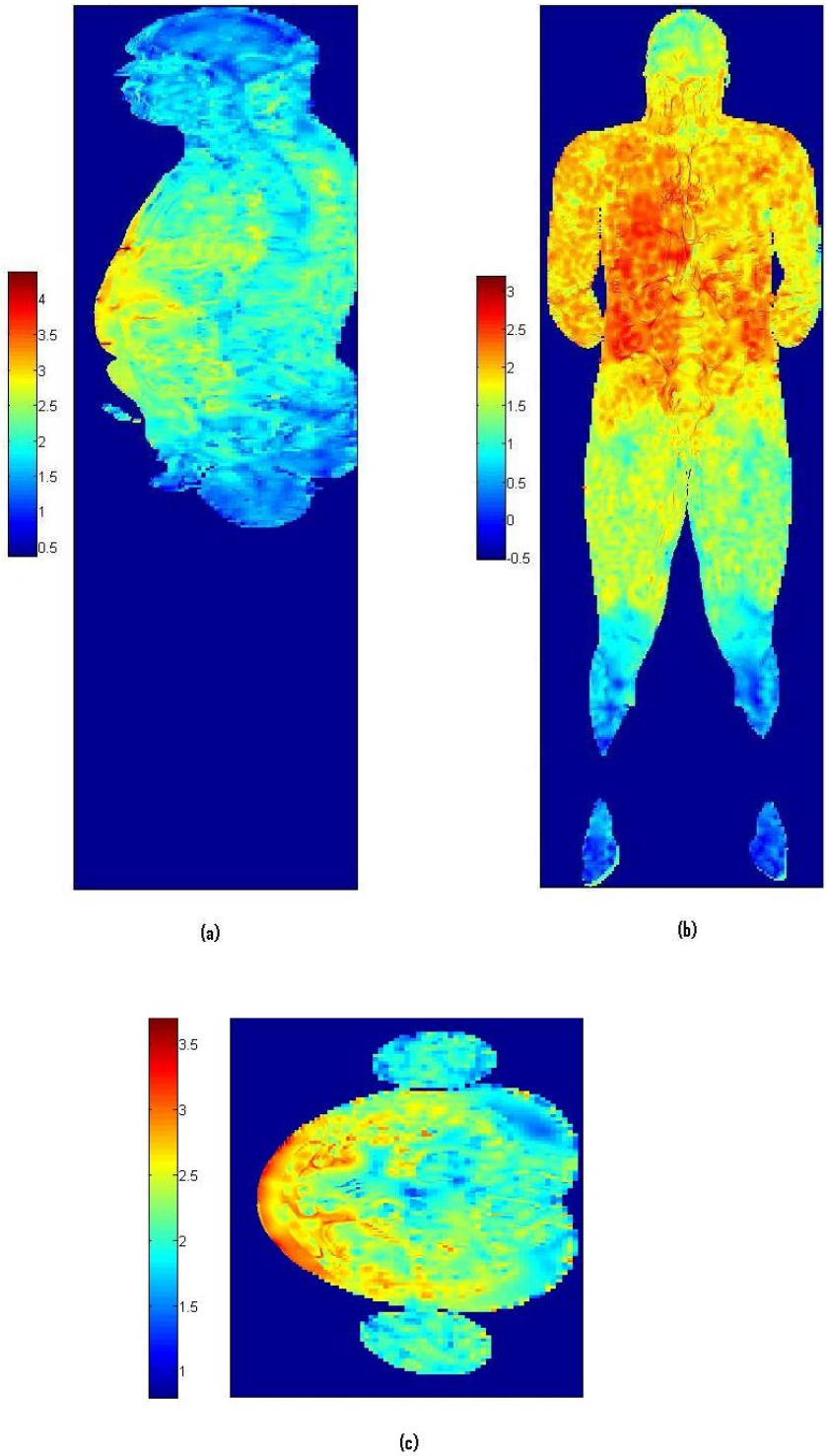

Figure 3.7: Electric fields (in $log_{10}(V/m)$) induces in the human body. (a) Sagittal view, (b) Coronal view and (c) transverse view. The source current magnitude is 500mA

Table 3.3: End mode recruitment volume divided amongst neurons of various diameters

Region	E field magnitude (Source current = 0.5A)	Recruitment volume (1000 cm^3)
	< 6.15 V/m	NA
	> 6.15 V/m but < 12.3 V/m	5.78
	> 12.3 V/m but < 24.6 V/m	10.88
	> 24.6 V/m but < 49.2 V/m	21.5
	> 49.2 V/m	59.7

To calculate the end mode recruitment volume, the volumes in the human body were identified where the electric fields exceeded the threshold values required for excitation as reported in [4]. Typically, these threshold values are inversely proportional to the diameter of the neurons and to the duration of the stimulation. Fig. 3.8 depicts the distribution of end mode recruitment volumes in the human body. The measure of these volumes and their corresponding recruitment thresholds are mentioned in table 3.3. A total of almost 98,000 cm^3 of human body is recruited. Most of the torso is heavily coupled. Only lower legs are not covered by the recruitment volume.

3.2.3 Center mode recruitment volume computation

Neurons can also be recruited if the gradient of the electric field along the length of a neuron exceeds the nerve excitation threshold. These thresholds too are inversely proportional to the diameter of a neuron and to the stimulation duration. Since the gradient along the direction of a neuron only can excite the neuron, only the following field gradients were computed:

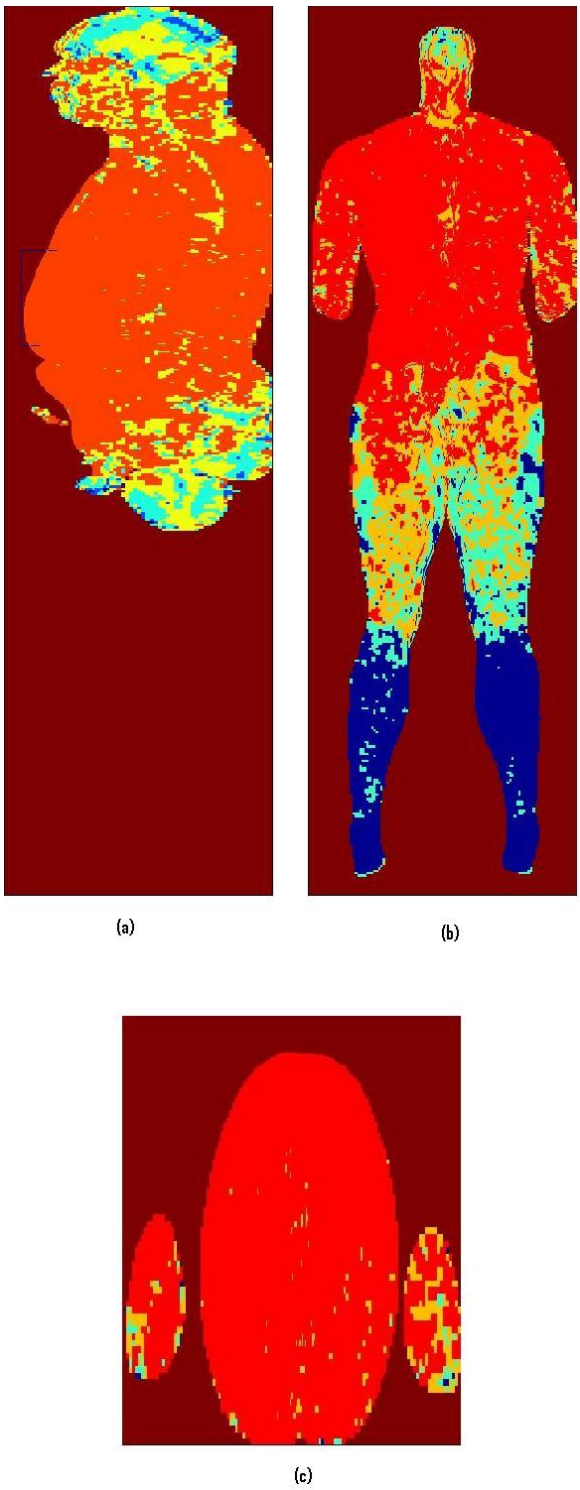

Figure 3.8: End mode recruitment volumes divided amongst various electric field thresholds. All values are for a current of 500mA flowing through the electrodes.

Table 3.4: Center mode recruitment volume divided amongst neurons of various diameters

Region	E field gradient (Source current = 0.5A)	Recruitment volume (1000 cm^3)
	< 1500 V/m^2	NA
	> 1500 V/m^2 but < 6000 V/m^2	34.4
	> 6000 V/m^2 but < 24000 V/m^2	29.8
	> 24000 V/m^2 but < 96000 V/m^2	10.9
	> 96000 V/m^2	5.09

$$\begin{aligned}\frac{\partial E}{\partial x} &= \frac{E(i,j,k) - E(i-1,j,k)}{\Delta x}\\ \frac{\partial E}{\partial y} &= \frac{E(i,j,k) - E(i,j-1,k)}{\Delta y}\\ \frac{\partial E}{\partial z} &= \frac{E(i,j,k) - E(i,j,k-1)}{\Delta z}\end{aligned} \tag{3.3}$$

An observation point inside the body is included in the center mode recruitment volume if any of the gradient values in equations 3.3 exceed the nerve excitation thresholds. The distribution of center mode recruitment volumes inside the human body is depicted in fig. 3.9 while table 3.4 details the threshold gradient values along with the measure of the recruitment volumes. Almost 80,000 cm^3 of the human body was recruited, which is less than the center mode recruitment volume.

3.3 Recruitment volume for magnetic stimulation

3.3.1 Computation of induced fields

The magnetic excitation was given through two circular coils with currents flowing in opposite directions. This allowed magnetic field lines to enter through one coil and

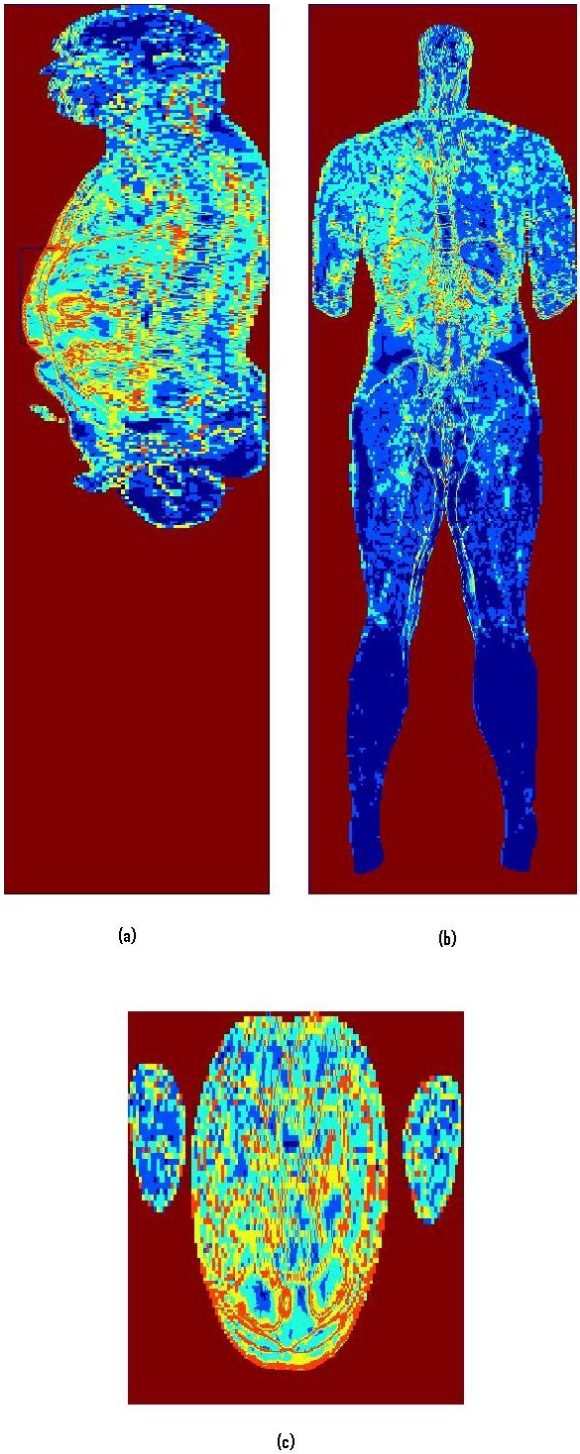

Figure 3.9: Center mode recruitment volume divided amongst various electric field gradient thresholds. All values are for a current of 500mA flowing through the electrodes.

exit through the other. The simulation was run for single turn coils as the fields can be easily scaled up for any number of turns. The diameter of the coils was arbitrarily set to 16mm as the fields can be scaled for any change in the coil area too. Since the induced fields magnitudes are directly proportional to the rate of change of current through the coils, maximum value of induced fields are computed for the body and are normalized with respect to the maximum rate of change in the source current. Building up of 8kA of current by capacitors with a rise time of mere 200μs has been reported [29]. The normalized fields were hence scaled up by a factor of $8kA/200\mu s = 40 \times 10^6 A/s$. To obtain appreciable recruitment volumes, the fields are further scaled up by another factor of 2000. This can correspond to 100 turn coils of around 7cm diameter.

The induced fields are shown in fig. 3.10. The fields are maximum in the area of the body nearest to the coils as expected. It can be noted that for the given setup, the field magnitudes are much lesser than those due to electrical stimulation.

3.3.2 End mode recruitment volume computation

The recruitment volumes for end mode excitation for magnetic source were computed in the same manner as they were computed for electrical stimulation is section 3.2.2, that is by identifying the volumes where electrical fields exceed nerve excitation thresholds. Fig. 3.11 shows the distribution of the recruitment volumes corresponding to different electric field thresholds. The values of these thresholds and the measure of the recruitment volumes are detailed in table 3.5. A total of just 43 cm^3 of human body is recruited. This is in sharp contrast to what was observed for electrical stimulation as the end mode recruitment volume for magnetic stimulation is almost negligible.

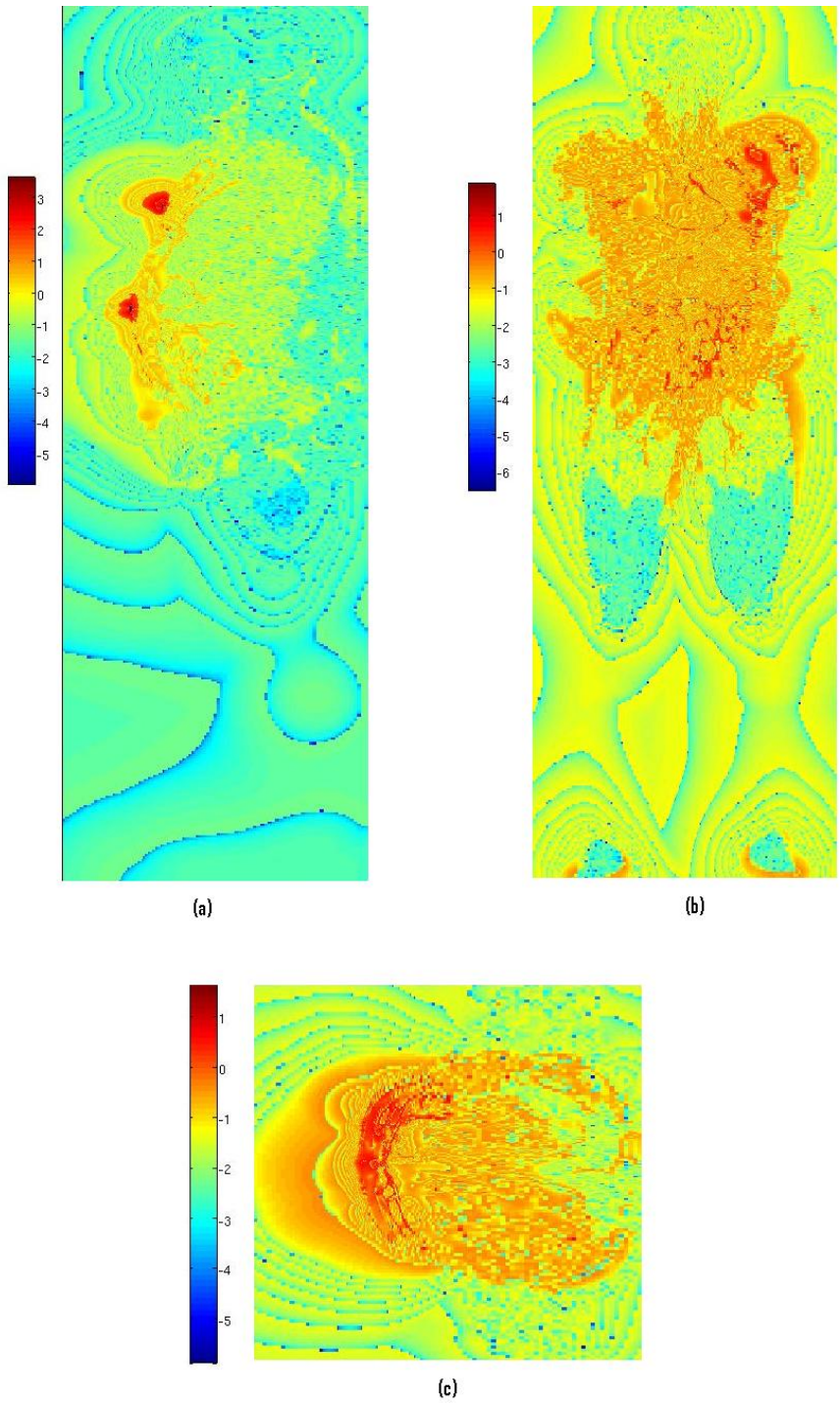

Figure 3.10: Electric fields (in $log_{10}(V/m)$) induces in the human body due to magnetic stimulation. (a) Sagittal view, (b) Coronal view and (c) transverse view.

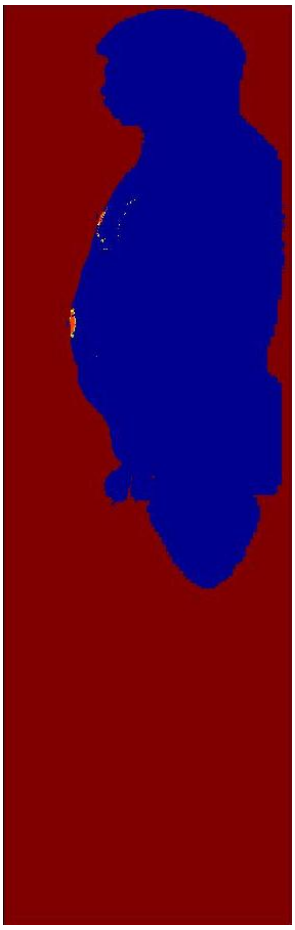

Figure 3.11: End mode recruitment volumes for magnetic stimulation divided amongst various electric field thresholds.

Table 3.5: End mode recruitment volume divided amongst neurons of various diameters

Region	E field magnitude (Source current = 0.5A)	Recruitment volume (cm^3)
	< 6.15 V/m	NA
	> 6.15 V/m but < 12.3 V/m	0
	> 12.3 V/m but < 24.6 V/m	0
	> 24.6 V/m but < 49.2 V/m	14
	> 49.2 V/m	29

Table 3.6: Center mode recruitment volume for magnetic stimulation divided amongst neurons of various diameters

Region	E field gradient (Source current = 0.5A)	Recruitment volume (cm^3)
	< 1500 V/m^2	NA
	> 1500 V/m^2 but < 6000 V/m^2	1373
	> 6000 V/m^2 but < 24000 V/m^2	4
	> 24000 V/m^2 but < 96000 V/m^2	44
	> 96000 V/m^2	7

3.3.3 Center mode recruitment volume computation

As mentioned in section 3.2.3, center mode recruitment volumes correspond to the volumes in the human body where the electric fields gradients along the length of the neurons are more than corresponding nerve excitation thresholds. The gradients are again computed using the equations in (3.3).

The distribution of center mode recruitment volumes inside the human body due to magnetic stimulation is shown in fig. 3.12. The measure of recruitment volumes and the corresponding gradient threshold values are detailed in table 3.6 . Almost 1428 cm^3 of the human body is recruited. Though this is much smaller than the center mode recruitment volume for electrical stimulation, it is much more than the end mode recruitment volume due to magnetic stimulation. It is conspicuous that for magnetic stimulation, center mode is the main mode for neuron excitation, while it is the other way round for electrical stimulation.

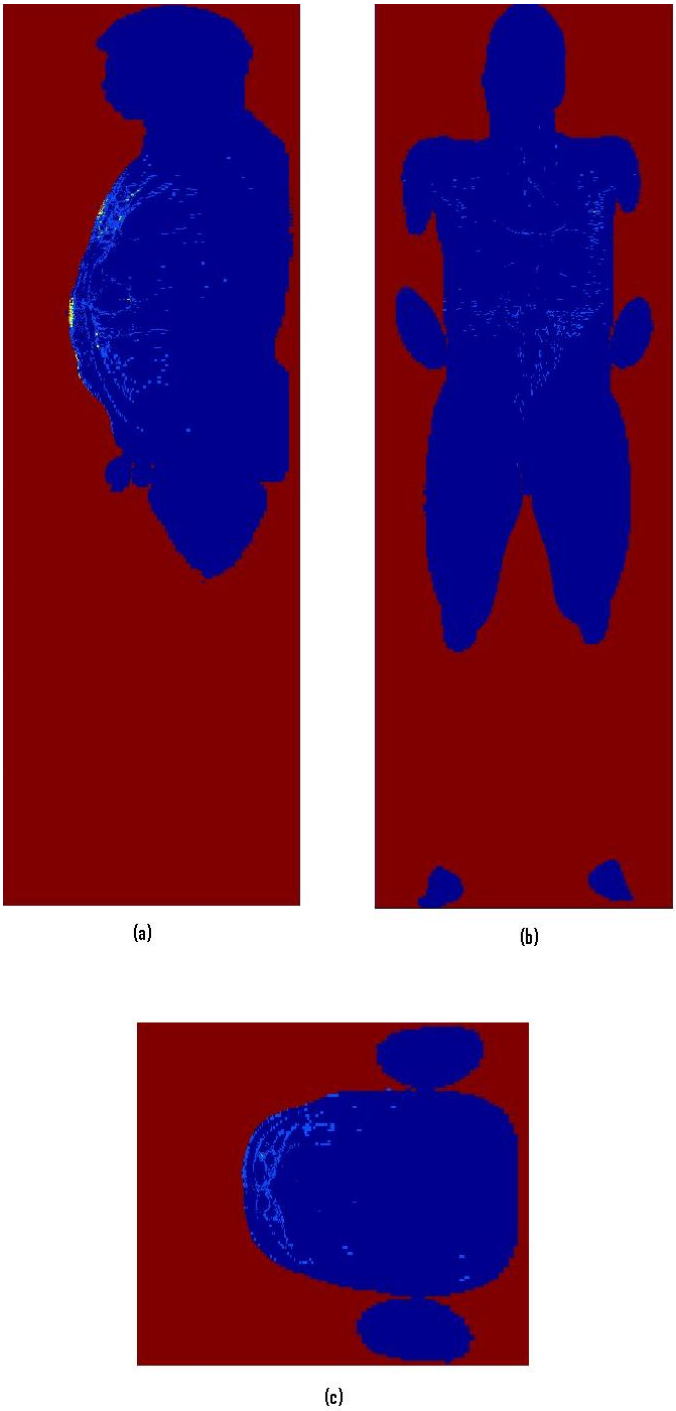

Figure 3.12: Center mode recruitment volume for magnetic stimulation divided amongst various electric field gradient thresholds.

Chapter 4

Conclusion and Future Work

In this work, end mode and center mode recruitment volumes inside a human body due to external electrical and magnetic stimulation are computed. The large size of the underlying full human body model could make the field-computation unacceptably slow. This situation could worsen for electric stimulation due to its low frequency source. ADI-FDTD method with expanding grid technique and quasi static assumption was employed to solve this problem within a tractable time range.

A CFL number of 16 used for the ADI-FDTD method was observed to decrease the simulation time by a factor of 5. The base human body model used was discretized at 1mm resolution. Through expanding grid techniques, this resolution was retained for only those parts of the model which were close to the source. The resolution was gradually increased to 5mm on moving away from the source. This way, the size of the computation models was decreased by around 90%. For the source waveform, a gaussian pulse with frequency contents up to several 100KHz was used. For the electrical stimulation, DFT averaging was performed for required frequencies over time durations much smaller than the corresponding time periods. Using quasi static assumptions, response for any source waveform can be reconstructed by appropriately

scaling responses due to the constituent frequencies.

For electrical stimulation, the end mode recruitment volume of almost 98,000 cm^3 was computed which covered almost the whole of the body except the lower legs. In almost half of the recruitment volume, neurons of all diameters appeared to be recruited. The center mode recruitment volume was found to be almost 80,000 cm^3. The volumes were mainly concentrated in the torso region. The DC resistance offered by the body for electrodes of $1mm^2$ cross sectional area penetrating about 10mm into the body was calculated to be 1.84kΩ.

The recruitment volumes for magnetic stimulations were found to be much lesser in measure. The end mode recruitment volume measured to be a negligible $43cm^3$ while the center mode recruitment volume was almost $1428cm^3$. It was also observed that the end-mode excitation was the main mode for neural excitation with electric stimulation while center-mode excitation was the main mode for neural excitation with magnetic stimulation.

Future work could include studying the effect of electrode size, positioning and penetration into the body. The frequency dependence of the dielectric properties of body tissue can also be incorporated into the solution. The quantification of the effect of CFL number on the accuracy of solution can also be studied.

Bibliography

[1] D. Panescu, "Design and medical safety of neuromuscular incapacitation devices," *IEEE Engineering in Medicine and Biology Magazine*, vol. 26, pp. 57–67.

[2] M. W. Kroll and P. Tchou, "How a taser works," *IEEE Spectrum Magazine*, Dec 2007.

[3] S. J. Holden, R. D. Sheridan, T. J. Coffey, R. A. Scaramuzza, and P. Diamantopoulos, "Electromagnetic modeling of current flow in the heart from taser devices and the risk of cardiac dysrhythmias," *Physics in Medicine and Biology*, vol. 52, pp. 7193–7209, 2007.

[4] J. P. Reilly, A. M. Diamant, J. Comeaux, "Dosimetery considerations for electrical stun devices", *Physics in Medicine and Biology*, vol. 54, no. 5, pp. 1319–1335, 2009.

[5] J. R. Jauchem, "Effectiveness and health effects of electro-muscular incapacitating devices", *Non-Lethal Technology and Academic Research Symp.*, 2004.

[6] Medical College of Wisconsin. MRI safety manual for researchers and staff. [Online]. Available: http://www.mcw.edu/FileLibrary/Groups/Biophysics/mrisafety/MRISafetyManual.pdf

[7] O. Gandhi and J. Y. Chen, "Numerical dosimetry at power line frequencies using anatomically based models," *Bioelectromagnetics Journal Supp.*, pp. 43–60, 1992.

[8] W. Xi, M. Stuchly, and O. Gandhi, "Induced electric currents in models of mand and rodents from 60 hz magnetic fields," *IEEE Transaction on Biomedical Engineering*, pp. 1018–1023, 1994.

[9] T. Dawson and M. Stuchly, "High-resolution organ dosimetry for human exposure to low-frequencymagnetic fields," *IEEE Transaction on Magnetics*, vol. 34, pp. 708–718, May 1998.

[10] S. Garcia, T. Lee, and S.Hagness, "On the accuracy of the adi-fdtd method," *IEEE Antennas and Wireless Propagation Letters*, vol. 1, pp. 31–34, 2002.

[11] V. Singh, Ajeet, G. Lazzi, "Computation of induced fields in the Human Torso at Low frequencies due to contact electrodes using the ADI-FDTD Method", *IEEE App. Electromagnetics Conf*, Kolkatta, India, Dec 19–20, 2007.

[12] A. Taflove and S. C. Hagness, *Computational Electrodynamics : The Finite-Difference Time-Domain Method*, 2nd ed. Artech House Publishers, 2000.

[13] R. F. Harrington, *Field computation by moment methods:IEEE Press Series on Electromagnetic Wave Theory*, 3rd ed. Wiley-IEEE Press, 1996.

[14] K. S. Yee, "Numerical solution of initial boundary value problems involving maxwell's equations in isotropic media," *IEEE Transactions Antenna and Propagation*, vol. 14, pp. 302–307, 1966.

[15] R. Holland, "Implicit three-dimensional finite differencing of maxwell's equations," *IEEE Trans. Nuclear Science*, vol. NS-31, pp. 1322–1326, 1984.

[16] F. Zheng, Z. Chen, and J. Zhang, "Towards the development of a three-dimensional unconditionally stable finite-difference time domain method," *IEEE Transactions Microwave Theory and Techniques*, vol. 48, pp. 1550–1558, 2000.

[17] J. P. Berenger, "A perfectly matched layer for the absorption of electromagnetic waves," *Journal of Computational Physics*, vol. 114, pp. 185–200, 1994.

[18] G. Lazzi, "Unconditionally stable d-h fdtd formulation with anisotropic pml boundary conditions," *IEEE Microwave and Wireless Components Letter*, vol. 11, no. 4, pp. 149–151, 2001.

[19] D. M. Sullivan, *Electromagnetic Simulation Using the FDTD Method*, 1st ed. Wiley-IEEE Press, 2000.

[20] Z. S. Sacks, D. M. Kingsland, R. Lee, and J.-F. Lee, "A perfectly matched anisotropic absorber for use as an absorbing boundary condition," *IEEE Transactions Antenna and Propagation*, vol. 43, no. 12, pp. 1460–1463, December 1995.

[21] S. Schmidt and G. Lazzi, "An improved pml formulation for the unconditionally stable d-h adi-fdtd method," *IEEE Antenna and Propagation International Symp.*, vol. 1, pp. 337–340, 2003.

[22] D. M. Sullivan, "A simplified PML for the use with FDTD method", in *IEEE IEEE Microwave and Guided Wave Letters*, vol. 6, no. 2, Feb 1996.

[23] B.-Q. Gao and O. P. Gandhi, "An expanding-grid algorithm for the finite-difference time-domain method," *IEEE Transactions On Electromagnetic Compatibility*, vol. 34, no. 3, pp. 277–283, 1992.

[24] M. E. Potter, M. Okoniewski, and M. A. Stuchly, "Low frequency finite difference time domain (fdtd) for modeling of induced fields in humans close to line sources," *Computational Physics*, vol. 162,, pp. 82–103, 2000.

[25] Ajeet., "Using the ADI-FDTD method to compute currents induced in the human body by HEMI devices at low frequencies." MS dissertation, North Carolina State University, 2008.

[26] S. Schmidt, C. J. Cela, V. Singh, J. D. Weiland, M. S. Humayun, G. Lazzi, "Computational modeling of electromagnetic and thermal effects for a dual-unit retinal prosthesis", *Artificial Sight*,Ed: M. S. Humayun, J. D. Weiland, G. Chader, E. Greenbaum (Springer/AIP Press), 2007.

[27] P. Mason, J. Ziriax, W. Hurt, and J. D'Andrea, "3-dimensional models for emf dosimetry," *Electricity and Magnetism in Biology and Medicine*, vol. 162,, pp. 291–294, 1999.

[28] I. N. R. Council. Dielectri properties of body tissue. [Online]. Available: http://niremf.ifac.cnr.it/tissprop/

[29] V. Walsh, A. Cowey, "Transcranial magnetic stimulation and cognitive neuroscience",in *Nat. Rev. Neurosci.*, vol. 1, pp. 7379, 2000.

[30] H. Sun, J. Y. Wu, R. Abdallah, and J. G. Webster, "Electromuscular incapacitating device safety," in *IFMBE*, vol. 11(1), Nov 2005.

[31] Wikipedia. Computational electromagnetics. [Online]. Available: http://en.wikipedia.org/wiki/Electromagnetic_modeling

[32] P. P. Silvester and R. L. Ferrari, *Finite elements for electrical engineers*, 3rd ed. New York: Cambridge University Press, 1996.

[33] T. Namiki, "A new fdtd algorithm based on alternating based on alternating-direction implicit method," *IEEE Transactions Microwave Theory and Techniques*, vol. 47, pp. 2003–2007, 1999.

[34] G. Lazzi, "Ece 540 class notes: The finite difference time domain method," NC State University, Raleigh, NC.

[35] T. Namiki, "3-d adifdtd methodunconditionally stable time-domain algorithm for solving full vector maxwells equations," *IEEE Transactions Microwave Theory and Techniques*, vol. 48, no. 10, pp. 1743–1748, October 2000.

[36] G. Liu and S. D. Gedney, "Perfectly matched layer media for an unconditionally stable three-dimensional adi-fdtd method," *IEEE MICROWAVE AND GUIDED WAVE LETTERS*, vol. 10, no. 7, pp. 261–263, July 2000.

[37] ——, "Extension and validation of a perfectly matched layer for the unconditionally stable d-h fdtd method," *IEEE Microwave and Wireless Components Letter*, vol. 13, no. 8, pp. 345–347, 2003.

[38] S. Schmidt, "Finite-difference time-domain methods for electromagnetic problems involving biological bodies." Ph.D. dissertation, North Carolina State University, 2005.

[39] F. Zheng and Z. Chen, "Numerical dispersion analysis of the unconditionally stable 3-d adi-fdtd method," *IEEE Transactions on Microwave Theory and Techniques*, no. 8.

[40] T. Dawson, J. Moerloose, and M. Stuchly, "Hybrid finite-difference method for high-resolution modeling for low frequency electric induction in humans," *Journal of Computational Physics*, vol. 136, pp. 640–653, 1997.

[41] C. M. Furse and . P. Gandhi, "Calculation of electric fields and currents induced in a millimeter-resolution human model at 60 hz using the fdtd method with a novel time-to-frequency-domain conversion," *Antennas and Propagation Society International Symposium*, vol. 3, pp. 1798–1801, 1996.

[42] M. Stuchly and T. Dawson, "Interaction of low-frequency electric and magnetic fields with the human body," in *Proceedings of the IEEE*, vol. 88, May 2000, pp. 643–664.

[43] S. Garcia, A. Bretones, R. Martin, and S. Hagness, "Accurate implementation of current sources in the adi-fdtd scheme," *IEEE Microwave Wireless Comp. Lett*, pp. 141–144, 2004.

[44] T.-W. Lee and S. C. Hagness, "Wave source conditions for the unconditionally stable adi-fdtd method," in *IEEE Antennas and Propagation Society Int. Symp.*, vol. 4, July.

[45] S. Gedney, "An anisotropic pml absorbing media for fdtd simulation of fields in lossy dispersive media," *Electromagnetics*, pp. 399–415, 1996.

[46] T. Dawson, K. Caputa, M. Stuchly, and R. Kavet, "Electric fields in the human body resulting from 60-hz contact currents," *IEEE Transaction Biomedical Engineering*, 2001.